

Incorporation of Contracture Formation during Dermal Wound Healing: a Mathematical Model

W. M. Boon

Technische Universiteit Delft

INCORPORATION OF CONTRACTURE FORMATION DURING DERMAL WOUND HEALING: A MATHEMATICAL MODEL

by

W. M. Boon

in partial fulfillment of the requirements for the degree of

Master of Science

in Applied Mathematics

at the Delft University of Technology,

to be defended publicly on June 2nd, 2014.

Student number: 1518046

Supervisor: Dr. ir. J. E. Vermolen, TU Delft

Thesis committee: Prof. dr. ir. C. Vuik, TU Delft

Dr. ir. J. H. Dubbeldam, TU Delft

Guest member: D. Koppenol, MSc TU Delft

An electronic version of this thesis is available at <http://repository.tudelft.nl/>.

ABSTRACT

In order to rapidly close skin wounds and prevent further infection, the process of contraction is initiated during wound healing. However, this process has the potential to become problematic as it may result in permanent contraction, or contracture formation. In order to give an insight in the dynamics involved with this process, we present a mathematical model of dermal wound healing which incorporates the contraction process and the possibility to develop a contracture as a consequence of wound healing. We consider various prominent mediators in the wound healing process and model the influences that each of these mediators has on each other and their surroundings. Using the model, we find that the number of myofibroblasts and the forces they exert on their surroundings are important factors in the degree of contracture formation.

Keywords: Contraction, Myofibroblasts, Transforming growth factor- β , Collagen synthesis.

CONTENTS

List of Figures	vii
List of Symbols	xi
Acknowledgments	xiii
1 Introduction	1
1.1 The Biological Process of Dermal Wound Healing	2
1.2 Prior Mathematical Modeling Work.	3
1.3 Setup of the Thesis	5
2 Mathematical Model	7
2.1 Biological Model	7
2.1.1 Mediators	8
2.1.2 Fibrin Decay	9
2.1.3 The Chemoattractant PDGF	11
2.1.4 Leukocyte Response	12
2.1.5 TGF- β Production	17
2.1.6 Fibroblast Response	18
2.1.7 Collagen Synthesis	19
2.1.8 Collagen Guidance	21
2.1.9 Cell Death	21
2.1.10 Overview	22
2.2 Mechanical model	23
2.2.1 Deformation	23
2.2.2 Boundary conditions.	25
2.2.3 Weak Formulation	25
2.2.4 Contractile Forces	26
2.2.5 Incorporation of a Moving Mesh	32
3 Numerical Implementation	35
3.1 Domain	35
3.2 Initial Conditions.	36
3.3 Finite Element Method	37
3.3.1 Fibrin Decay	37
3.3.2 Collagen Synthesis	41
3.3.3 Contraction	42

3.4	Interaction between continuum and discrete entities	43
3.5	Time Integration Scheme	44
4	Results and Discussion	47
4.1	Fibrin Dynamics	48
4.2	Cytokine Production	50
4.3	Cell Populations	53
4.4	Collagen Synthesis	55
4.5	Contraction	58
4.6	Cell movement	59
4.7	Increase in Temporary Forces	62
4.8	Increase in Plastic Forces	63
5	Conclusions	65
6	Recommendations	67
	Bibliography	69
A	Lists of Parameters	71

LIST OF FIGURES

2.1	The domain representing a cross section of the upper part of the skin. A wound area is defined at the top of the domain which is surrounded by undamaged tissue.	7
2.2	The initial fibrin-rich clot modeled using a product of hyperbolic tangents as shown in equation (2.2). We assume a high concentration of fibrin in the wound space and nearly zero in the surrounding, undamaged tissue.	9
2.3	The initial distribution of PDGF which has a high concentration in the wound space. .	12
2.4	Cell velocity scaling factor depending on proportion of bound PDGF receptors.	15
2.5	In the model of Cumming et al. (2010), a collision causes the direction to change with a minimal deviation.	17
2.6	In this model, a different approach is used whenever two cells overlap. In order to account for contact forces, a repelling displacement is calculated using the size of h . .	17
2.7	A simplified representation of the direct influences of the main mediators on each other. The dashed lines imply that only the velocity is affected.	23
2.8	Temporary forces on a square curve around the center.	29
2.9	Dividing the circular area of influence into five equal pieces. The five points are used to approximate the overlapping area between the myofibroblast and an element. . . .	30
2.10	The three directions of the plastic forces for an element.	31
2.11	Directions of plastic forces in all elements. By increasing the artificial time τ for different elements, the corresponding forces are increased.	32
3.1	The original domain of computation used in Cumming et al. (2010) showing the wound space at the top surrounded by undamaged tissue and the four boundaries.	36
3.2	Adjusted domain since we consider wounds with different proportions. The width of the wound is now larger than its depth.	36
3.3	Triangular mesh on the domain of computation. Note that the mesh is denser near the boundary of the wound space and the top boundary.	37
4.1	The average fibrin density within the domain of computation throughout time. Note that the fibrin-rich clot which initially occupies the wound space, is removed during the first 10 days of the wound healing process.	48
4.2	The dynamics of the fibrin density at consecutive times in a single model run. We see that the clot is broken down from the wound edges towards the center of the wound. .	49
4.3	The average PDGF concentration within the domain of computation throughout time. Note that this cytokine slowly diffuses into the surrounding, undamaged tissue in order to attract leukocytes.	50

4.4	The dynamics in PDGF concentration throughout time. The cytokine quickly diffuses from the wound site into the surrounding tissue in order to attract leukocytes.	51
4.5	The 5 th percentile, mean and 95 th percentile at each time step of 100 simulations. We see that the deviation from the mean only concerns the height of the peak and not the moment in time at which it occurs.	52
4.6	The TGF- β profile throughout time shows that the peak, which occurs at approximately day 5, lies within the wound space.	52
4.7	The number of leukocytes and fibroblasts in the wound space throughout time. The distinction between two phases in the process is made by noting which cell species forms the majority.	53
4.8	The 5 th percentile, mean and 95 th percentile of the number of leukocytes and fibroblasts in the wound space at each time step. The deviation concerning the fibroblast population is significantly larger than the deviation in leukocyte population. Nevertheless, the two peaks marking the different stages of wound healing can be seen clearly.	54
4.9	The 5 th percentile, mean and 95 th percentile of the average collagen density in the domain during each time step. The highest increase in collagen density occurs once the fibrin clot is broken down and the first fibroblasts arrive.	55
4.10	The collagen density in the domain throughout time. The wound site is filled with collagen fibers synthesized by fibroblasts and myofibroblasts which arrive from the surrounding tissue. After 300 hours, some lighter areas can be seen which mark a lower collagen density. This is mostly due to the lower collagen synthesis by arriving (myo)fibroblasts.	56
4.11	The anisotropy of collagen bundles in the domain throughout time. A large difference can be seen between the isotropic tissue in blue which surrounds the wound area and the newly formed collagen fibers in the wound area which are shown in red due to anisotropy.	57
4.12	The anisotropy of collagen bundles in the domain throughout time.	58
4.13	The 5 th percentile, mean and 95 th percentile of the area of the wound space during each time step. A small, initial increase can be seen due to contractile forces outside the wound space. This is followed by a large decrease in area as fibroblasts enter the wound space, produce collagen and exert both temporary and plastic forces here. Finally, the contracture can be seen by the constant area in the final stages of the simulation.	59
4.14	Cell positions, orientation of collagen fibers and the borders of the domain and wound space consecutive times. Fibroblasts and myofibroblasts and leukocytes are represented in blue and red, respectively. Collagen fibers are shown in black in which the crosses are aligned with the eigenvectors of the tensor.	60
4.15	A typical final state of the domain after three weeks. Note that the contracture is shown here since it remains after all other processes are completed. Furthermore, the difference in isotropy in collagen bundles can be seen between the wound space and the surrounding tissue.	61

-
- 4.16 If the temporary forces are increased, the initial decrease of the wound area is greater. However, once the (myo)fibroblasts start to decay, the area increases to a steady state. 62
- 4.17 If the plastic forces are increased, the degree of contraction is increased as well. In this case, the plastic forces seem to completely dominate the temporary forces. 63

LIST OF SYMBOLS

Symbol	Description
ϕ_t	tPA concentration which is responsible for the decay of fibrin.
ϕ_P	PDGF concentration: the chemoattractant for leukocytes.
ϕ_T	TGF- β concentration: the chemoattractant for fibroblasts produced by leukocytes.
ρ_f	Fibrin density.
ρ_c	Collagen density.
$\underline{\underline{\Psi}}$	Collagen tensor.
φ	Test function from $\mathcal{H}^1(\Omega)$.
\underline{x}_c	Cell coordinates.
\underline{x}_p	Mesh point coordinates.
n	Proportion of bound receptors on a cell.
n_f	Total number of (myo)fibroblasts.
N_l	Total number of leukocytes.
n_{mp}	Number of force points from (myo)fibroblasts.
n_p	Number of mesh points.
n_e	Number of triangular elements.
n_l	Number of line elements.
\underline{n}	Normal vector.
Ω	Stationary domain of computation.
Ω_t	Dynamic domain of computation.
Ω_t^n	Dynamic domain of computation at time t_n .
Ω_w	Wound space.
Γ_w	Boundary between the wound space and the surrounding tissue.
Ω_c	Area occupied by a cell.
Ω_e	Triangular element e .
l_j	Linear element j .
e_j	Node j on triangular element e .

ACKNOWLEDGMENTS

Under the daily supervision of Fred Vermolen and Daniël Koppenol, I spent approximately nine months working on the research presented in this thesis. I would like to express my gratitude towards both for their continuous support, enthusiasm, and belief in this work. First, I would like to thank Fred for his commitment to this project and for sharing his creative thoughts and ideas during the course of this research. In particular, his contributions were essential in the mathematical formulation of contracture formation. Second, I would like to thank Daniël for freely sharing his knowledge and skills concerning the biological process of dermal wound healing and the numerical analysis required in its implementation. Whenever questions arose, he was always available for answers and guidance and I greatly appreciate his helpfulness.

1

INTRODUCTION

Dermal wound healing is a process which consists of a highly orchestrated, partly overlapping sequence of events (Mutsaers et al., 1997). As the wound heals in different stages, various mediators are responsible for different components in this process. In order to correctly initiate and complete the events necessary for skin restoration, these mediators are in a constant relationship with each other. These relationships make wound healing a highly complex process. By mathematically formulating the behavior of a selection of the prominent mediators and their influences on each other, we present a model which simulates some of the sub-process involved in wound healing.

A notable sub-process which takes place during dermal wound healing is contraction. (Midwood et al., 2004) During this process, the damaged tissue gets pulled together in order to close the wound rapidly and minimize the chance of infection. Naturally, this is a desirable effect for wounds, but when the contraction is too abundant, it can become a negative side-effect. In that case, a permanent contraction known as a contracture can be the result. This may lead to problems such as functional restrictions (Enoch and Leaper, 2008).

A major difference between scar tissue and undamaged tissue lies in the alignment of its fibers (Cumming et al., 2010). While undamaged tissue has an isotropic pattern of interwoven collagen bundles, scar tissue is characterized by fibers aligned in only a few directions. This anisotropy causes the tissue to have inferior strength and flexibility. Clark (2014) and Murphy et al. (2012) state that the regenerated tissue has only 70% of the normal dermal strength. Furthermore, the reduction in flexibility can cause major problems for the affected patient (Hinz, 2006).

Because of the great implications that contraction has on the final stages of skin repair, it serves as an interesting component in a wound healing model. By combining the mechanical implications due to contraction with some of the biological processes of dermal wound healing, we aim at creating a more complete view of the entire wound healing process. Such a model may lead to a better understanding of the wound healing process which is essential for the development of new

procedures to reduce contracture formation in the resulting scar tissue.

1.1. THE BIOLOGICAL PROCESS OF DERMAL WOUND HEALING

In order to establish a view of the most important components in the healing process, some of the mediators and the different sub-processes are introduced here. As introduced by Enoch and Leaper (2008), the wound healing process can be divided into four main stages called haemostasis, inflammation, proliferation and remodeling. Even though these phases overlap partly, they are well-defined and together form the entire process from the initiation of the wound to the final scar tissue. We present a short description of each of these stages and focus on the components relevant to the model. For further information, a more detailed description can be found in Enoch and Leaper (2008) and Clark (2014).

HAEMOSTASIS

The first stage, called the haemostasis stage is initiated immediately after wounding. In this stage, blood coagulates to form a clot made up of fibrin and fibronectin at the wound site in order to stop excessive blood loss (Midwood et al., 2004). This clot acts as a growth factor reservoir (Clark, 2014) and includes the growth factor Platelet-Derived Growth Factor (PDGF). This growth factors is highly involved in the wound healing cascade by attracting leukocytes, fibroblasts, and endothelial cells. (Enoch and Leaper, 2008)

INFLAMMATION

The inflammation stage takes place in the first 3 days after wounding. Within 24-48 hours (Enoch and Leaper, 2008), leukocytes infiltrate the wound and start to phagocytose bacteria and other foreign particles. The leukocytes which have entered the wound start producing chemoattractants which aid in the attraction of fibroblasts (Murphy et al., 2012), the main cell type in dermal repair. These chemoattractants include the well-known Transforming Growth Factor- β (TGF- β) (Enoch and Leaper, 2008), which has various effects on fibroblasts including stimulation to migration and proliferation (Clark, 2014).

In reaction to the blood clot, the production of a cytokine named tissue Plasminogen Activator (tPA) is also initiated at the edge of the wound during the first days of wound healing. This results in the breakdown of the fibrin clot and the subsequent production of granulation tissue. this granulation tissue consists of blood vessels, leukocytes, fibroblasts and loose connective tissue (Mutsaers et al., 1997).

PROLIFERATION

After approximately 3 days, the arrival of the first fibroblasts marks the start of the proliferation stage (Enoch and Leaper, 2008). This stage lasts for 2-4 weeks after wounding. As mentioned before, these cells are attracted towards the wound by a number of factors including the TGF- β . After arrival to

the wound site, fibroblasts then start to proliferate and may differentiate into myofibroblasts, a type of fibroblast with smooth muscle cell characteristics (Murphy et al., 2012).

Fibroblasts and myofibroblasts are the primary factors involved in the process of contraction. In this process, the cells adhere to the surrounding medium through which it moves, called the extracellular matrix (or ECM). The ECM is comprised mostly of collagen fibrils (Enoch and Leaper, 2008). They then pull together these collagen fibrils and consequently compact the connective tissue (Clark, 2014). The difference between the cells is that myofibroblasts will exert stronger contractile forces than fibroblasts (Hinz, 2006). An abundance of contraction may result in the permanent contraction (i.e. the contracture) of the wound which remains after all fibroblasts and myofibroblasts have either died or left the wound area.

Furthermore, both fibroblasts and myofibroblasts will initiate the synthesis of the oriented collagen fibrils in the wound. These form the building blocks for the new ECM which replaces the fibrin clot. These collagen fibrils themselves act as a guidance cue for subsequently arriving fibroblasts. Hence, there is a constant interaction where fibroblasts affect the orientation of the collagen matrix and the orientation of this collagen matrix influences the movement of fibroblasts (McDougall et al., 2006).

REMODELING

The final stage of wound healing, called the remodeling stage, mostly consists of the continued interaction between fibroblasts and collagen. The extracellular matrix is constantly remodeled as fibroblasts synthesize and reorient collagen fibrils. Meanwhile, the continued contraction process brings the wound margins closer together and hence further decreases the size of the wound. (Enoch and Leaper, 2008).

As the scar matures, the remodeling serves to gain tensile strength in the wound (Enoch and Leaper, 2008). During the third week however, the collagen deposition has slowed down significantly and the remaining gain in strength is achieved by connecting different collagen bundles (Clark, 2014). After several months, the tensile strength of the wound has been increased from approximately 20% to 70% of normal dermal strength (Clark, 2014; Murphy et al., 2012).

1.2. PRIOR MATHEMATICAL MODELING WORK

Since there is an extensive amount of literature available on the mathematical modeling of dermal wound healing, we will limit our review to the most relevant articles for the present work. Hence we focus on articles concerning the mathematical modeling of the contraction process and the orientation of the collagen bundles in the dermis during dermal wound healing.

In the field of wound contraction modeling, Tranquillo and Murray (1992) were one of the first to propose a mathematical model for wound healing that takes the contraction process into account. The model presented in this work offered a general framework for understanding how traction exerted by wound fibroblast eventually results in wound contraction. The equations described here formed the basis for much of the computational research in this field.

From this model, the model by Olsen and colleagues (1995; 1996) followed. They formulated a deterministic mathematical model in order to investigate key clinical problems in wound healing disorders. The focus was on contraction and simplifications were made such that only the essential roles of fibroblasts and myofibroblasts were described along with a single chemical growth factor and the ECM. The results showed that a distinction needed to be made between contraction during the proliferation stage and the prolonged remodeling of collagen during the remodeling stage.

Another significant contribution to this field was the model by Murphy et al. (2012). This model incorporated the interaction between fibroblasts and the ECM combined with a more realistic modeling of cytokines. Contraction was investigated in a one-dimensional model activated by TGF- β . Here, the cytokine and mechanical tension were assumed to be responsible for the differentiation from fibroblast to myofibroblast. The model then showed that the removal of TGF- β and reduction of tension resulted in a decrease in the number of myofibroblasts and therewith a reduction in contraction. A major shortcoming of these early works, however, is that a contracture is not a stable solution within these models.

With respect to the dynamics of fiber bundle orientation, one of the most important mathematical theories was formulated by Barocas and Tranquillo (1997). In this work, an anisotropic biphasic theory for tissue-equivalent mechanics was presented. This theory can account for fibril alignment during wound healing and introduced cell contact guidance. Although the theory was formulated in a general sense, it was speculated that it may be valid for physiological processes such as wound contraction (Barocas and Tranquillo, 1997).

Later, the dynamics of fiber bundle orientation was incorporated into a dermal wound healing model by Olsen et al. (1999). Here, two approaches were proposed for modeling the cell populations. First, the cell densities were modeled as continua. This continuum approach resulted in a system of partial differential equation on a macroscopic scale. However, patterns of alignment on microscopic length scales were lost in this approach. Therefore, a novel approach was introduced in which cells are presented as discrete individuals and the ECM as a continuum. This hybrid model produced the desired results on both scales.

The modeling of the interaction between cells and the ECM alignment was developed further by Dallon and colleagues (2000; 1999; 2001) by including ECM production and decay. In all cases, the cells were considered as discrete objects while the matrix was modeled as a continuum. In Dallon et al. (1999), various aspects of the cell interactions with collagen and fibrin were investigated first in order to find which alignment properties arise in different cases. These aspects included cell speed, flux, polarization, density, initial matrix orientation and the influence of cells on the matrix. The results showed that all of these factors had a certain effect on the alignment of collagen. It was shown next by Dallon et al. (2000) that of these factors, cell speed and the positions where fibroblasts enter the wound area are the most influential on fiber alignment. Within the model, the matrix orientation was modeled using a vector field. This implied that the orientation of the bundles was unidirectional.

In a third article, Dallon and colleagues (2001) incorporated a time-variant concentration field for

the cytokine TGF- β to the model and the effects of different profiles of this cytokine were investigated. It was found that the influence TGF- β has on changes in cell motility, proliferation and collagen production had little effect on collagen matrix alignment. Furthermore, it was shown that the alignment of the new tissue depends highly on the fibroblast reorientation rate.

A couple of years later, a further investigation was conducted by McDougall and colleagues (2006) on the effects of different cytokine concentrations. They made an important distinction between the degree of scarring and wound integrity. It was shown that a large chemoattractant diffusion coefficient results in an optimized wound integrity while the degree of scarring is decreased when a competitive inhibitor to TGF- β is introduced.

From the vector-based representations of collagen bundles and fibrin fibers used by Dallan et al. (1999) and McDougall et al. (2006), a few drawbacks can easily be deduced. First, there is no measure available for the degree of isotropy of the field at a point. Second, a vector-based approach is unidirectional while fiber bundle alignment works in a bidirectional manner. In order to overcome both these limitations, Cumming and colleagues (2006; 2010) have presented a tensorial approach to collagen bundle orientation based on the earlier work of Barocas and Tranquillo (1997).

The model presented by Cumming and colleagues (2010) further incorporated several of the main biological sub-processes which make up the dermal wound healing process. The model was particularly extensive since a total of six species were incorporated ranging from discrete cells to the continuum tensorial approach of the ECM. This model will serve as a basis for this project and is explained extensively in Section 2.1.

1.3. SETUP OF THE THESIS

In this thesis, we present a mathematical model for dermal wound healing which incorporates both some of the most relevant biological entities, the orientation of the collagen bundles, and the mechanical process of contraction. In Chapter 2, the different biological mediators and the corresponding governing equations are presented first. We elaborate on the different assumptions and choices made within the model and discuss several adjustments. Next, we formulate the incorporation of the contraction process in the model in a mathematical sense.

The algorithm for the numerical analysis of the model is presented in Chapter 3. We elaborate on several key components including the numerical scheme used to solve the partial differential equations. Furthermore, we discuss some challenges in implementation of the algorithm which are a consequence of the complexity of the model.

The results obtained from the model are presented in Chapter 4. The behavior of the different components in the model is demonstrated and we discuss the implications of the results. Furthermore, we focus on the progress of contraction throughout the wound healing process and the different effects this extension has on the biological model.

Chapter 5 contains the conclusions derived from this work. Here, we reflect on our initial goal of

incorporating the contraction process and contracture in a dermal wound healing model. Finally, recommendations for future research are presented in Chapter 6.

2

MATHEMATICAL MODEL

In this chapter we elaborate on the different components of the mathematical model. First, we formulate the biological processes and mediators that are included in the model in a mathematical manner. The basis of this part of the model is a framework which was derived earlier by Cumming et al. (2010). The governing equations that were derived in that framework are re-evaluated and adjusted whenever necessary. Second, we derive the equations that describe the mechanics involved in the process of contraction during dermal wound healing. Finally, the mathematical formulation of this extension is presented as well.

2.1. BIOLOGICAL MODEL

Let us consider a cross-section of the upper part of the skin, such that the top represents the skin surface. We then define a region at the top of the domain which represents the wound space as shown in Figure 2.1.

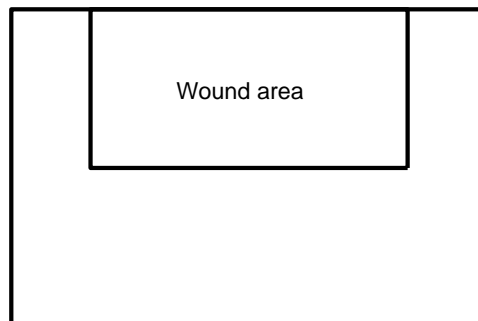


Figure 2.1: The domain representing a cross section of the upper part of the skin. A wound area is defined at the top of the domain which is surrounded by undamaged tissue.

In this section, we introduce the various mediators that are taken into account and the way in which they are modeled mathematically. Subsequently, we elaborate on the different interspecies influences by chronologically considering the different stages of the wound healing process.

2.1.1. MEDIATORS

In order to fully understand the mathematical model, we introduce the responsible mediators. By considering their behavior and the way they are modeled, we classify them into three types, namely cells, cytokines and fibers.

CELLS

The cells are implemented as discrete entities moving through the dermis similar to the model introduced by Dallon et al. (1999). In this model, we limit the number of cell species to two, namely fibroblasts and leukocytes. These cells are represented by discs with a radius r_c such that the location of their centers define the position of the cell. Leukocytes are responsible for producing cytokines which attract both fibroblasts and their activated form: myofibroblasts.

Both fibroblasts and myofibroblasts synthesize and reorient collagen bundles. Furthermore, they exert forces on their surrounding tissue causing contraction. In this model, we assume that myofibroblasts cause contracture in the later stages of the wound healing process. Since the behavior of fibroblasts and myofibroblasts only differs in the process of contraction, the way in which they are modeled is primarily the same. In order to model the difference during the process of contraction, each cell is accompanied by a label to identify whether it is a fibroblast or myofibroblast.

In addition, each cell has a number of receptors which are bound to its corresponding cytokine. The number of bound receptors has a direct influence on the behavior of the cell.

CYTOKINES

The cytokines are responsible for fibrin decay and attracting the different cell species to the wound space. These concentrations are modeled as continuum entities subject to partial differential equations. We limit ourselves to three species of cytokine, namely tPA for fibrin decay, PDGF for leukocyte attraction, and TGF- β for the attraction of (myo)fibroblasts.

FIBERS

The two fiber species in this model are collagen and fibrin. While the fibrin density only plays a role in the inflammatory phase, the density of collagen bundles plays a prominent role throughout the wound healing process. These densities influence cytokine diffusion, cell movement and the magnitude of contractile forces. Furthermore, the orientation of collagen bundles guides (myo)fibroblasts towards the wound space.

2.1.2. FIBRIN DECAY

At the start of the model, we assume that the fibrin-rich clot is completely formed. The first step in the model is then to simulate the breakdown of this clot. Even though the fibrin density influences several factors, its decay is influenced by the concentration of one cytokine, namely tissue Plasminogen Activator (tPA). In short, a higher concentration of tPA results in a faster degradation of the fibrin clot.

We denote the fibrin density and tPA concentration by ρ_f and ϕ_t , respectively. With the use of a degradation factor r_p , we model this breakdown using the following formula:

$$\frac{\partial \rho_f}{\partial t} = -r_p \phi_t \rho_f. \quad (2.1)$$

In order to find a unique solution to this differential equation, an initial condition is required. The fibrin-rich clot which initially fills the wound space at the top of the domain is modeled by assuming that the fibrin density is high in the wound space and zero in the surrounding tissue. We use hyperbolic tangents to describe this initial function ρ_f^0 so that discontinuities can be avoided:

$$\rho_f^0(x, y) = \frac{1}{8} [1 + \tanh(5(2 - x))] [1 + \tanh(5(2 + x))] [1 + \tanh(5y)]. \quad (2.2)$$

A visualization of this initial profile is shown in Figure 2.2.

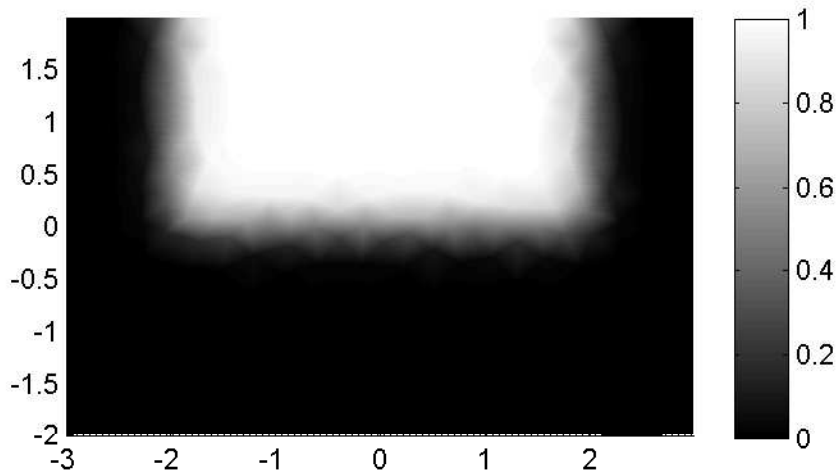


Figure 2.2: The initial fibrin-rich clot modeled using a product of hyperbolic tangents as shown in equation (2.2). We assume a high concentration of fibrin in the wound space and nearly zero in the surrounding, undamaged tissue.

After the formulation of the influence of the tPA concentration on the fibrin density, we consider the converse effect. The tPA spreads throughout the domain through the process of diffusion which is modeled using a diffusion equation. Since the cytokine diffuses much slower in the fibrin clot than in undamaged tissue, we adjust the diffusion equation to incorporate this effect. This is modeled mathematically by making the diffusion coefficient depend on the fibrin density. Furthermore, a

source term T_t is added to represent the production of tPA along the wound edge. The differential equation which describes the dynamics of tPA is then formulated as follows:

$$\frac{\partial \phi_t}{\partial t} = \nabla \cdot (D(\rho_f) \nabla \phi_t) + T_t. \quad (2.3)$$

For simplicity, we assume a linear decrease in diffusion from the maximum D_{max} to the minimum D_{min} as the fibrin density increases from zero to unity:

$$D(\rho_f) = D_{max}(1 - \rho_f) + \rho_f D_{min}. \quad (2.4)$$

The source term T_t is high along the borders of the wound space and zero in the rest of the domain. In Cumming et al. (2010), this is modeled using a discontinuous function in which a border area along the wound boundary is defined. However, an extra uncertainty arises when declaring the width of this area. Furthermore, the addition of a mechanical component in the model will cause this area to distort creating extra difficulties in implementation.

In order to avoid these difficulties, we have chosen to change the source function such that tPA is produced only on the boundary Γ_w between the wound area and the surrounding area comprised of undamaged tissue. Let us consider the following function $\delta_\Gamma(\underline{x})$:

$$\delta_\Gamma(\underline{x}) \begin{cases} = 0, & \underline{x} \notin \Gamma. \\ > 0, & \underline{x} \in \Gamma. \end{cases} \quad (2.5)$$

Such that

$$\int_Q \delta_\Gamma(\underline{x}) \, d\Omega = \frac{\mu(\Gamma \cap Q)}{\mu(\Gamma)}, \quad \text{for } Q \subseteq \Omega, \quad (2.6)$$

in which $\mu(\Gamma)$ represents the length of Γ .

The following formula then describes the production of tPA in which s_t represents the total amount of tPA produced per unit of time:

$$T_t(\underline{x}) = s_t \delta_{\Gamma_w}(\underline{x}). \quad (2.7)$$

Note that T_t is independent of time. The only influence tPA has in this model is in the process of fibrin decay. Therefore, once the fibrin clot has decayed, this production term no longer has an effect on the rest of the model. For simplicity, we assume a constant production as this avoids introducing unnecessary parameters with respect to time.

Equation (2.3) now requires an initial condition and a set of boundary conditions. At the moment of wounding, there is no tPA present in the domain which means that we impose the following initial condition:

$$\phi_t = 0, \text{ at } t = 0. \quad (2.8)$$

For the boundary conditions, we consider the physical meaning of each of the boundaries. The upper (or north) boundary (Γ^N) represents the surface of the skin. Naturally, the cytokine should

not be able to diffuse out of the domain at this boundary, so a no-flux condition is imposed:

$$\left. \frac{\partial \phi_t}{\partial \underline{n}} \right|_{\Gamma^N} = 0. \quad (2.9)$$

With \underline{n} the unit normal vector pointing out from the boundary. The remaining boundaries (Γ^E , Γ^S , and Γ^W) are assumed to border on undamaged tissue in which no tPA is present. The boundary condition that needs to be imposed here should enable the cytokine concentration to diffuse out of the domain freely. The amount of diffusion should be balanced by the transport in the undamaged tissue over the long range. This amount is given by $\kappa_t(0 - \phi_t)$ since the concentration should be zero far away. Hence, we get the following Robin condition:

$$\left. \frac{\partial \phi_t}{\partial \underline{n}} \right|_{\Gamma^E \cup \Gamma^S \cup \Gamma^W} = -\kappa_t \phi_t, \quad \kappa_t > 0. \quad (2.10)$$

Taken together, the dynamics of the tPA concentration are described by the following PDE accompanied by initial and boundary conditions:

$$\begin{cases} \frac{\partial \phi_t}{\partial t} = \nabla \cdot (D(\rho_f) \nabla \phi_t) + T_t, & \text{in } \Omega, \\ \frac{\partial \phi_t}{\partial \underline{n}} = 0, & \text{on } \Gamma^N, \\ \frac{\partial \phi_t}{\partial \underline{n}} = -\kappa_t \phi_t, & \text{on } \Gamma^E \cup \Gamma^S \cup \Gamma^W, \\ \phi_t = 0, & \text{at } t = 0. \end{cases} \quad (2.11)$$

2.1.3. THE CHEMOATTRACTANT PDGF

The next phase in the healing process is marked by the arrival of leukocytes. Amongst other factors, these cells are attracted towards the wound space by high concentrations of various chemoattractants. In Cumming et al. (2010), these chemoattractants are simplified to a single cytokine, namely Transforming Growth Factor- β (TGF- β). However, since these leukocytes also produce this cytokine, they will start to cluster in areas with a high concentration that they have created themselves. This becomes apparent after running numerical simulations.

The simplification to a single chemoattractant therefore leads to unrealistic behavior. In this model, we create a distinction between the cytokine produced by leukocytes and its chemoattractant. Out of the various cytokines which serve as chemoattractants, we choose Platelet-Derived Growth Factor (PDGF) to fulfill this role.

The dynamics of the concentration of PDGF is modeled with the use of the diffusion equation in a way similar to equation (2.3). A few simplifications can be made since it is assumed that there is no production of PDGF, only an initially high concentration inside the wound space. The PDGF will then diffuse into the surrounding tissue so that its gradient will point back towards the wound space. This gradient will serve as a guidance cue for the leukocytes.

It is assumed that the PDGF concentration is high within the wound space and nearly zero outside.

Once more, this is accomplished using the same product of hyperbolic tangents as in equation (2.2). Figure 2.3 shows a plot of the initial distribution of PDGF.

$$\phi_P^0(x, y) = \frac{1}{8} [1 + \tanh(5(2 - x))] [1 + \tanh(5(2 + x))] [1 + \tanh(5y)]. \quad (2.12)$$

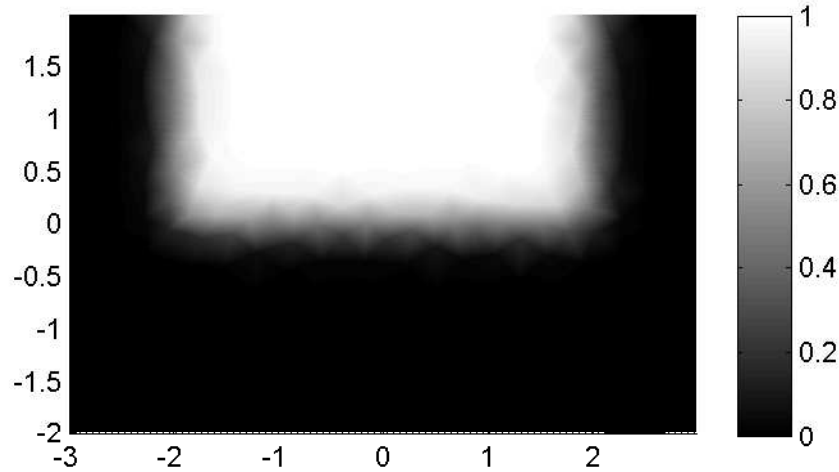


Figure 2.3: The initial distribution of PDGF which has a high concentration in the wound space.

Finally, we will assume a constant diffusion coefficient D_P in order to simplify the calculations. Furthermore, the same boundary conditions as for ϕ_t are used. Taken together, the dynamics of the PDGF concentration are described by the following PDE accompanied by initial and boundary conditions:

$$\begin{cases} \frac{\partial \phi_P}{\partial t} = \nabla \cdot (D_P \nabla \phi_P), & \text{in } \Omega, \\ \frac{\partial \phi_P}{\partial n} = 0, & \text{on } \Gamma^N, \\ \frac{\partial \phi_P}{\partial n} = -\kappa_P \phi_P, & \text{on } \Gamma^E \cup \Gamma^S \cup \Gamma^W, \quad \kappa_P > 0, \\ \phi_P = \phi_P^0, & \text{for } t = 0. \end{cases} \quad (2.13)$$

2.1.4. LEUKOCYTE RESPONSE

We distinguish the response leukocytes have to an increase in PDGF concentration into four consecutive processes. First, we consider the arrival of leukocytes in the wound domain. Second, we consider the process of binding PDGF-receptors which will trigger the cell's reaction. Third, the cell will start to move towards the center of the wound. This movement is described and finally the reaction due to contact forces is incorporated as well.

LEUKOCYTE ARRIVAL

In Cumming et al. (2010), the leukocytes are present in the surrounding undamaged tissue. The diffusion of PDGF then triggers the first leukocytes to migrate to the wound site. However, this way

of modeling seems unrealistic to us since the leukocytes should arrive through the blood stream (Clark, 2014).

In order to model this, we note that along the boundary between the wound space and the surrounding tissue, severed blood vessels can be found. Therefore we define this region as an area in which new leukocytes can be introduced to the model.

The number of leukocytes that enter in a certain time step and the exact location of entry are determined using stochastic variables which depend on the PDGF concentration. Let us consider a counting process $N(t)$ in the form of a Poisson process in order to determine how many cells enter the domain during the time step.

As explained by Ross (1996), a counting process $\{N(t), t \geq 0\}$ is said to be a Poisson process having rate λ , $\lambda > 0$, if it has the following three properties:

- i. $N(0) = 0$.
- ii. The process has independent increments.
- iii. The number of events in any interval of length t is Poisson distributed with mean λt . That is, for all $s, t \geq 0$:

$$\mathbb{P}(N(t+s) - N(s) = m) = e^{-\lambda t} \frac{(\lambda t)^m}{m!}. \quad (2.14)$$

With the use of the mean value of PDGF concentration on the wound boundary (ϕ_p^w) we propose the following for the rate λ :

$$\lambda = \beta \phi_p^w, \quad (2.15)$$

in which β is the average number of cells entering per unit of time when the PDGF concentration is at its maximum. Let us denote the number of cells entering within time t by N_t . Since we aim to find the number of cells arriving during the next time step, we obtain:

$$\mathbb{P}(N_{\Delta t} = m) = e^{-\beta \phi_p^w \Delta t} \frac{(\beta \phi_p^w \Delta t)^m}{m!}. \quad (2.16)$$

By using the properties of a Poisson distribution (Ross, 1996), the following expected value is obtained:

$$\mathbb{E}(N_{\Delta t}) = \lambda \Delta t = \beta \phi_p^w \Delta t. \quad (2.17)$$

Note that this means that the expected number of cells arriving within the time step increases whenever ϕ_p^w or Δt increases. This is a desired effect since a higher concentration of PDGF should attract more leukocytes and a larger time step provides more time for leukocytes to arrive in.

With the number of cells entering the domain, we require a position at which these cells can arrive. For simplicity, we consider a uniform distribution \underline{U} on the wound boundary Γ_w . This distribution has the following probability density function:

$$f_{\underline{U}}(\underline{x}) = \delta_{\Gamma_w}(\underline{x}), \quad \underline{x} \in \Omega, \quad (2.18)$$

in which $\delta_{\Gamma_w}(\underline{x})$ is defined as in equation (2.5). For each cell entering the domain, a sample is taken

from this distribution to determine its point of entry.

RECEPTOR BINDING

Once the leukocytes have arrived in the dermis, they will react to the concentration of PDGF in their surroundings. However, since these cells do not respond instantly, the model introduces receptors which can bind to this chemoattractant. This receptor-mediated approach has been investigated extensively by Haugh (2006).

In short, a cell will only react once its receptors are bound. The proportion of bound receptors (n) will be modeled according to the following differential equation:

$$\frac{\partial n}{\partial t} = -\beta_P n + \gamma_P \phi_P (1 - n), \quad \beta_P, \gamma_P > 0. \quad (2.19)$$

Here, β_P is the factor for the natural unbinding of receptors while γ_P is the factor for receptors binding to PDGF. The term $(1 - n)$ ensures that the proportion of bound receptors does not exceed unity. Note that as the PDGF concentration gradually decays in the later stages of the simulation, the cell receptors will unbind as well since the term $-\beta_P n$ will become more dominant. This implies that leukocytes will be less active in the later stages of the wound healing process, which is a desired effect.

In order to finalize this initial value problem, we will impose an initial condition. Since the cells have not been introduced to the cytokine at $t = 0$, we impose:

$$n(0) = 0. \quad (2.20)$$

MOVEMENT

The first effect of an increase in bound receptors is on the movement of leukocytes. As described in Cumming et al. (2010), the cells will be modeled as discrete discs moving through the mesh. Cell movement is then described by a combination of a (unit) direction vector and a scalar, describing the movement velocity. Cumming et al. (2010) give the following equation for the migration velocity:

$$v_l = v_{max}(1 - k_6 \rho_f)(1 - k_7 \rho_c) \left(\frac{1}{4} + \frac{3}{4 + 80(1 - n)^6} \right), \quad (2.21)$$

in which v_{max} is the maximum velocity, and k_6 and k_7 are constant parameters. Furthermore, ρ_c represents the collagen density. As this equation shows, the movement velocity declines linearly as the density of fibrin or collagen increases. This would indicate that once the fibrin clot has decayed, it is more difficult for a cell to move through undamaged tissue than through the damaged area.

As described by Enoch and Leaper (2008), the extracellular matrix, composed mostly of collagen fibrils, is a critical regulator in cell movement and supports further ingrowth of cells. Therefore, the absence of collagen should not increase the cell velocity. An adaptation to this term is therefore required.

In this adaptation, we take into account that the tissue in the upper layer of the dermis (called the papillary dermis) is comprised of loosely arranged collagen fibers (Lookingbill and Marks, 2000). With this in mind, we assume that the velocity of the cells should decrease as they move into the upper regions of the domain. The reason is that the cells will experience trouble to find rigid spots to adhere to in the loosely connected regions.

A third factor incorporates the effect that a higher proportion of bound PDGF receptors has on the cell velocity. This last dependency on bound receptors is shown in Figure 2.4. Taken together, we adjust equation (2.21) to obtain the following:

$$v_l = v_{max} \left(1 - e^{-\|\underline{x}_l - \Gamma^N\|_2}\right) (1 - k_6 \rho_f) \left(\frac{1}{4} + \frac{3}{4 + 80(1 - n)^6}\right). \quad (2.22)$$

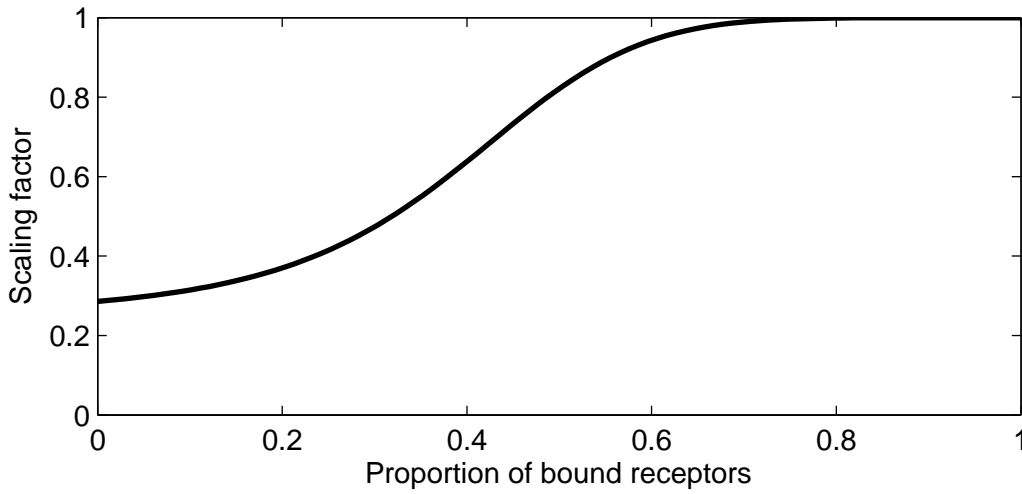


Figure 2.4: Cell velocity scaling factor depending on proportion of bound PDGF receptors.

For the second part of the cell movement, a (unit) direction is given. The leukocytes will move towards a higher concentration of PDGF. In Cumming et al. (2010), this direction \underline{g}_l , where the subscript l stands for leukocytes, is defined by a differential equation and then normalized if $\underline{g}_l \neq \underline{0}$:

$$d\underline{g}_l = (-\beta_l \underline{g}_l + \gamma_l (1 - n) \nabla \phi_P) dt + \sqrt{\alpha} dW. \quad (2.23)$$

First, β_l defines the directional persistence which is a measure for how quickly a cell is able to change direction. Then, γ_l is the sensitivity factor of the leukocytes movement to the gradient of the chemo-attractant ϕ_P . The influence of bound PDGF receptors is found in the term $1 - n$. It was chosen in order to model that as the number of bounded receptors increases, the cell becomes less aware of its surroundings and it becomes more difficult to sense the gradient of the corresponding cytokine. The last term in equation (2.23) describes a deviation in the form of a standard Wiener process with scaling factor $\sqrt{\alpha}$.

A standard Wiener process is defined in Ross (1996) as a stochastic process $[X(t), t \geq 0]$ with the following three properties:

- i. $X(0) = 0$,
- ii. $\{X(t), t \geq 0\}$ has stationary independent increments,
- iii. for every $t > 0$, $X(t)$ is normally distributed with mean 0 and variance t .

Note that with the multiplication of the factor $\sqrt{\alpha}$, the variance of the last term in equation (2.23) becomes αt .

This approach does have one disadvantage. Since the vector \underline{g}_l is normalized in each time step, the norm of the gradient of ϕ_P has no influence on the velocity. It is more reasonable if the cells slow down as the experienced gradient goes to zero as this would imply that they are approaching the center of the wound. Because of the decomposition into a velocity size and unit vector, this effect is not incorporated. For this reason, we will use a different approach in which the normalization of \underline{g}_l is adjusted.

$$d\underline{x}_l = v_l \gamma_l (1 - n) \frac{\nabla \phi_P}{1 + \|\nabla \phi_P\|} dt + \sqrt{\alpha} dW. \quad (2.24)$$

Now, the displacement is strongly dependent on the gradient of the PDGF-concentration. Note however, that the directional persistence has been neglected in this formulation.

In conclusion, the cell positions \underline{x}_l are updated as follows:

$$\underline{x}_l^{i+1} = \underline{x}_l^i + d\underline{x}_l. \quad (2.25)$$

CONTACT FORCES

Since the cells in this model are described as discrete individuals, an adjustment needs to be made once a collision happens. One way to make this adjustment is presented in Cumming et al. (2010) in which a new direction is chosen such that the deviation from its original path is minimal. This approach is illustrated in Figure 2.5. Such a direction can always be chosen except in the special case where the angle θ equals $\pm \frac{1}{2}\pi$ which means that the cell has a ‘head-on’ collision and is forced to stop.

Even though this technique seems to work well with small time steps, it fails when the time steps get bigger. Since ‘head-on’ collisions occur quite often as cells group together, cells are forced to stop even though they could push the blocking cells out of the way. To improve this part of the model, we will use the contact mechanical model Vermolen and Gefen (2012) in which contact forces are formulated. These forces will push cells away from each other once they start to overlap. Using this approach, a much more realistic view can be made for the way in which groups of cells move.

In order to account for these contact forces, the distance is calculated between the different cells after the position update in (2.25). For overlapping cells, the resulting force is calculated by finding the vector between the cell positions. Using these vectors, the corresponding contact forces are calculated and the cell positions are updated once again.

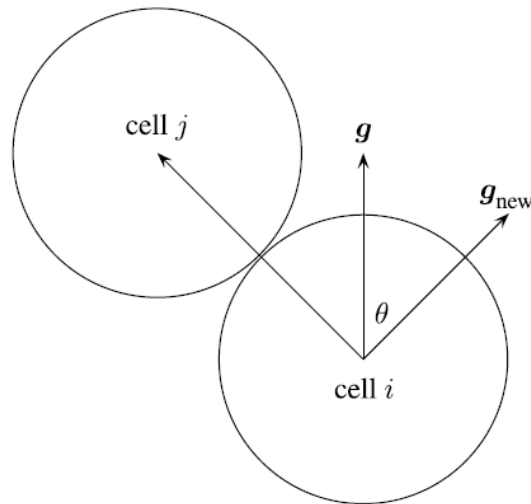


Figure 2.5: In the model of Cumming et al. (2010), a collision causes the direction to change with a minimal deviation.

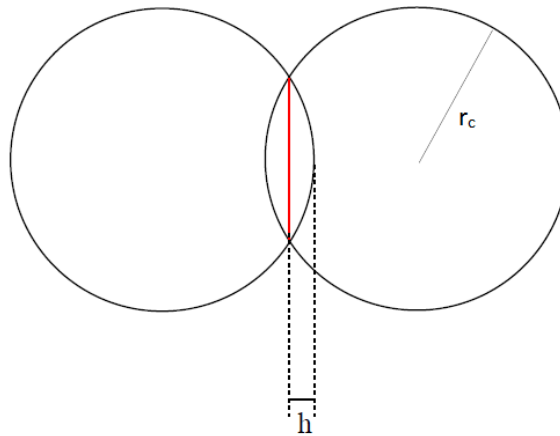


Figure 2.6: In this model, a different approach is used whenever two cells overlap. In order to account for contact forces, a repelling displacement is calculated using the size of h .

2.1.5. TGF- β PRODUCTION

Besides moving towards the center of the wound, leukocytes respond to an increase in PDGF concentration by producing Transforming Growth Factor- β (TGF- β). Analogous to the concentration of tPA described in 2.3, the concentration of this cytokine ρ_T will be modeled using a diffusion equation:

$$\frac{\partial \phi_T}{\partial t} = \nabla \cdot (D(\rho_f) \nabla \phi_T) + T_T. \quad (2.26)$$

In this case, the source function represents the production of the cytokine by leukocytes which we model as point sources using Dirac delta functions. The main factor for producing TGF- β is contact with fibrin (ρ_{f_i}) since this indicates that the cell has reached the wound space. Taken together, the

source term becomes:

$$T_T(\underline{x}, t) = c_{max} \sum_{i=1}^{N_l} [(1 - \rho_{f_i})c_{fib} + \rho_{f_i}] \cdot \delta(\underline{x} - \underline{x}_i^l), \quad (2.27)$$

in which we use the parameters c_{max} for the maximum production, c_{fib} for the influence of fibrin density, and N_l for the total number of leukocytes.

In order to define an initial condition, we note that there is no TGF- β present in the domain in the beginning. Therefore, we impose:

$$\phi_T(\underline{x}, 0) = 0, \quad \text{for } \underline{x} \in \Omega. \quad (2.28)$$

Since this is a cytokine similar to tPA and PDGF, its behavior on the boundaries is the same as well. The boundary conditions imposed for this cytokine are therefore identical to the ones in equation (2.11):

$$\begin{cases} \frac{\partial \phi_T}{\partial n} = 0, & \text{on } \Gamma^N, \\ \frac{\partial \phi_T}{\partial n} = -\kappa_T \phi_T & \text{on } \Gamma^E \cup \Gamma^S \cup \Gamma^W, \quad \kappa_T > 0. \end{cases} \quad (2.29)$$

2.1.6. FIBROBLAST RESPONSE

As the concentration of TGF- β increases, more cell species are attracted towards the wound area, namely fibroblasts and myofibroblasts which are assumed to be present in the surrounding, undamaged tissue. Note that the distinction between fibroblasts and myofibroblasts is only made with respect to the process of contraction. Therefore, their behavior with respect to receptor binding and movement is identical.

The receptors on fibroblasts and myofibroblasts bind in the same manner as the PDGF-receptors on leukocytes. A small adaptation to equation (2.19) formulates the proportion of bound receptors on (myo)fibroblasts:

$$\frac{\partial n}{\partial t} = -\beta_T n + \gamma_T \phi_T (1 - n). \quad (2.30)$$

The equation which describes the movement of fibroblasts $d\underline{x}_f$ is the same as we have seen in Section 2.1.4 with one trivial difference. Since fibroblasts move towards higher concentrations of TGF- β , the term $\nabla \phi_P$ is replaced with $\nabla \phi_T$ in equation (2.24):

$$d\underline{x}_f = v_f \gamma_f (1 - n) \frac{\nabla \phi_T}{1 + \|\nabla \phi_T\|} dt + \sqrt{\alpha} d\underline{W}. \quad (2.31)$$

Here, the scalar v_f which describes the velocity is calculated analogous to equation (2.22).

A major difference between (myo)fibroblasts and leukocytes, however, is that (myo)fibroblasts proliferate once a minimum proportion of receptors n_{thres} stay bound for a certain period of time. For this purpose, a timer τ_f is created for each (myo)fibroblast which is updated according to the

following:

$$\tau_f^{i+1} = \tau_f^{i+1} + \begin{cases} \Delta t, & n^i > n_{thres}, \\ 0, & n^i \leq n_{thres}. \end{cases} \quad (2.32)$$

If τ_f exceeds a predefined τ_{max} , then the cell will be ready to proliferate. A second threshold needs to be exceeded, however, since the cell needs space in order to undergo the process of mitosis. By calculating the distance to nearby cells, the cell density is approximated and it is determined whether mitosis can occur.

If all proliferation criteria are met, the process of mitosis will create a new cell which is introduced at the same location as its parent. The calculated contact forces as described in Section 2.1.4 are then further responsible for removing the overlap.

2.1.7. COLLAGEN SYNTHESIS

For the implementation of collagen, the orientation is just as important as its density ρ_c . Therefore, Cumming et al. (2010) describes a tensor approach to the collagen fibers which will be denoted by $\underline{\underline{\Psi}}$. The advantage of this approach is that the density and orientation can be saved in one quantity. First, the collagen density equals the trace:

$$\rho_c = \text{tr}(\underline{\underline{\Psi}}) = \text{tr} \begin{bmatrix} \Psi_{xx} & \Psi_{xy} \\ \Psi_{xy} & \Psi_{yy} \end{bmatrix} = \Psi_{xx} + \Psi_{yy}. \quad (2.33)$$

Second, the eigenvectors of $\underline{\underline{\Psi}}$ define the orientation of the fibers and the corresponding eigenvalues determine the dominance of these fibers.

The tensor representation is then modeled to satisfy the following differential equation:

$$\frac{\partial \underline{\underline{\Psi}}}{\partial t} = (1 - \rho_f - \rho_c) \cdot \sum_{i=1}^{n_f} (k_2 n_i + k_1 (1 - n_i)) \cdot \underline{\underline{g}}_i \underline{\underline{g}}_i^T \cdot \mathbb{1}_c^i(\underline{\underline{x}}), \quad k_1, k_2 \geq 0 \quad (2.34)$$

The first factor ensures that the total density of fibrin and collagen does not exceed unity. Then a sum is made over all (myo)fibroblasts in which n_f represents the total number of (myo)fibroblasts. They will orient the collagen according to their own (normalized) movement direction $\underline{\underline{g}}_i$. The amount of collagen produced depends strongly on the proportion of bound TGF- β receptors the fibroblast has with k_1 and k_2 as the lower and upper limit, respectively.

Finally, the function $\mathbb{1}_c^i(\underline{\underline{x}})$ represents the indicator function which is defined as follows:

$$\mathbb{1}_c^i(\underline{\underline{x}}) = \begin{cases} 1, & \text{if } \underline{\underline{x}} \in \Omega_c^i \\ 0, & \text{if } \underline{\underline{x}} \notin \Omega_c^i \end{cases} \quad (2.35)$$

In which Ω_c^i is the area occupied by cell i . Let us now consider the dynamics of the collagen density

which is determined according to equation (2.33). First, let us write out the term $\underline{g}_i \underline{g}_i^T$:

$$\underline{g}_i \underline{g}_i^T = \begin{bmatrix} g_{i,x}^2 & g_{i,x} g_{i,y} \\ g_{i,x} g_{i,y} & g_{i,y}^2 \end{bmatrix}. \quad (2.36)$$

Furthermore, we denote the term concerning the rate of production by α_i :

$$\alpha_i = k_2 n_i + k_1 (1 - n_i). \quad (2.37)$$

We then consider the following:

$$\frac{\partial \Psi_{xx}}{\partial t} = (1 - \rho_f - \rho_c) \cdot \sum_{i=1}^{n_f} \alpha_i \cdot g_{i,x}^2 \cdot \mathbb{1}_c^i(\underline{x}), \quad (2.38)$$

$$\frac{\partial \Psi_{yy}}{\partial t} = (1 - \rho_f - \rho_c) \cdot \sum_{i=1}^{n_f} \alpha_i \cdot g_{i,y}^2 \cdot \mathbb{1}_c^i(\underline{x}). \quad (2.39)$$

The sum of these two equations results in:

$$\begin{aligned} \frac{\partial(\Psi_{xx} + \Psi_{yy})}{\partial t} &= \frac{\partial \rho_c}{\partial t} = (1 - \rho_f - \rho_c) \cdot \sum_{i=1}^{n_f} \alpha_i \cdot (g_{i,x}^2 + g_{i,y}^2) \cdot \mathbb{1}_c^i(\underline{x}) \\ &= (1 - \rho_f - \rho_c) \cdot \sum_{i=1}^{n_f} \alpha_i \cdot \mathbb{1}_c^i(\underline{x}). \end{aligned} \quad (2.40)$$

Here, we used the fact that \underline{g}_i is a normalized vector. Since

$$\sum_{i=1}^{n_f} \alpha_i \cdot \mathbb{1}_c^i(\underline{x}) \geq 0, \quad (2.41)$$

we derive that $\rho_c = 1 - \rho_f$ is a stable equilibrium.

The initial condition for the collagen density is that the uninjured tissue consists of isotropically oriented collagen and there is no collagen present in the wound space. We use the derived equilibrium state to impose the following initial density ρ_c^0 :

$$\rho_c^0 = 1 - \rho_f^0. \quad (2.42)$$

Formulating the tensor which represents the fibers is then done by noting that the densities are stored in the trace and the medium is isotropic. Therefore, we arrive at the following initial condition $\underline{\Psi}^0$:

$$\underline{\Psi}^0 = \begin{bmatrix} \frac{1}{2} \rho_c^0 & 0 \\ 0 & \frac{1}{2} \rho_c^0 \end{bmatrix}, \quad (2.43)$$

keeping in mind that $\text{tr}(\underline{\Psi}) = \rho_c$.

2.1.8. COLLAGEN GUIDANCE

The orientation of the collagen fibers is generated in the direction towards the center of the wound. These bundles now serve a second purpose, namely to guide subsequently arriving fibroblasts in the same direction. This alteration depends on the collagen density ρ_c at the position of the cell. Contact guidance is represented in Cumming et al. (2010) by the following tensor multiplication:

$$\hat{\underline{\underline{g}}}_f = [(1 - \rho_c)\underline{\underline{I}} + \rho_c\underline{\underline{\Psi}}]\underline{\underline{g}}_f. \quad (2.44)$$

Here, $\underline{\underline{\Psi}}$ is the normalized (length-preserving) orientation tensor of collagen at the location of the fibroblast and $\underline{\underline{I}}$ is the 2×2 identity matrix. If the collagen density is zero, there is no contact guidance while a higher collagen density results in a higher influence on its direction.

To incorporate contact guidance, we use equation (2.31) and include contact guidance as formulated in equation (2.44). We then arrive at:

$$d\underline{\underline{x}}_f = v_f \gamma_f (1 - n) [(1 - \rho_c)\underline{\underline{I}} + \rho_c\underline{\underline{\Psi}}] \frac{\nabla \phi_T}{1 + \|\nabla \phi_T\|} dt + \sqrt{\alpha} d\underline{\underline{W}}. \quad (2.45)$$

In which v_f is calculated analogous to equation (2.22). Afterwards, the contact forces between cells are incorporated as explained in Section 2.1.4.

2.1.9. CELL DEATH

In order to control the cell populations, cell death is introduced as well which we model as a stochastic process. In order to do this, we use exponential distributions with a certain mean value μ . The cumulative distribution function is given by:

$$F_\mu(x) = 1 - e^{-\frac{x}{\mu}}. \quad (2.46)$$

For all cell types, a sample is taken from the exponential distribution (X) and then compared to Δt . If $X < \Delta t$, then the cell decays. Otherwise, it lives on until the next time step. Using the cumulative distribution function, we arrive at the following probability:

$$\mathbb{P}(\text{Cell dies during next time step}) = \mathbb{P}(X < \Delta t) = 1 - e^{-\frac{\Delta t}{\mu}}. \quad (2.47)$$

Let us now consider the value of μ for each cell type. For leukocytes, we assume the lifespan is highly dependent on the concentration of PDGF. We therefore define the following:

$$\mu_l = \phi_P \mu_l^{avg} \quad (2.48)$$

In which μ_l^{avg} is the average life span of a leukocyte in an environment with a high PDGF concentration. Note that since μ_l can now become zero when $\phi_P = 0$, a definition is required for the

probability of cell death if $\mu_l = 0$. Let us consider the following limit:

$$\lim_{\mu \downarrow 0} F_\mu(\Delta t) = \lim_{\mu \downarrow 0} 1 - e^{-\frac{\Delta t}{\mu}} = 1. \quad (2.49)$$

With this limit, we see that if $\mu_l = 0$, then the cell will decay almost surely during the subsequent time step. This implies that all leukocytes will decay when the PDGF concentration decreases to zero. Since this happens at the end of the wound healing process, this effect can be seen as apoptosis, or programmed cell death.

In the case of (myo)fibroblasts, such a relationship with its cytokine TGF- β is undesirable. TGF- β concentration is close to zero in the initial stages of the process, which would result in all (myo)fibroblasts decaying in the beginning. Therefore, a mean μ_f^{avg} representing the average lifespan of (myo)fibroblasts during wound healing is used.

$$\mu_f = \mu_f^{avg} \quad (2.50)$$

2.1.10. OVERVIEW

We have seen that the different mediators each play their own role in certain components of the model. In order to give an overview of the interspecies influences, Figure 2.7 gives a simplified representation. Now that the existing model has been evaluated and adjusted, the next step is the formulation and incorporation of contraction for which it is now suited.

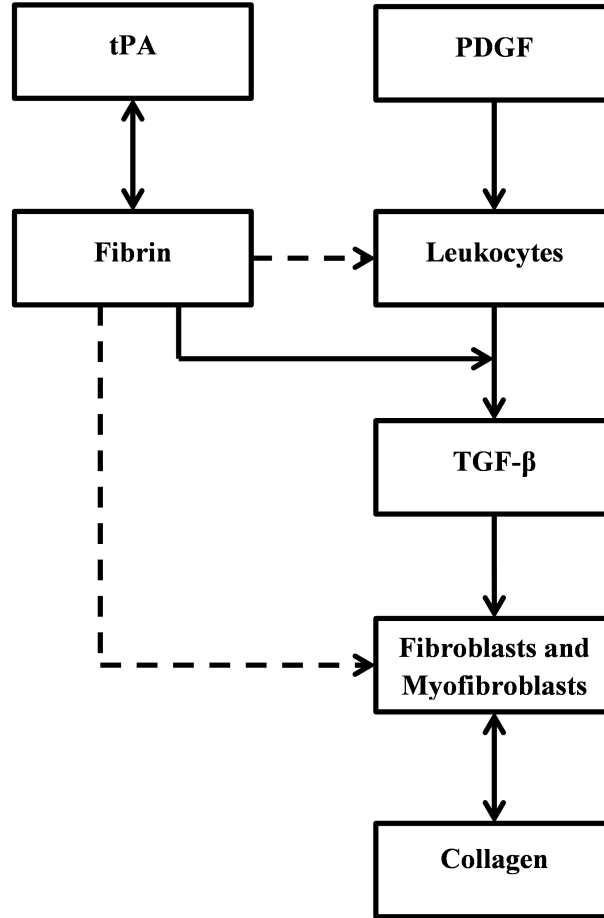


Figure 2.7: A simplified representation of the direct influences of the main mediators on each other. The dashed lines imply that only the velocity is affected.

2.2. MECHANICAL MODEL

The main addition to the model is the incorporation of contractile forces by fibroblasts and myofibroblasts. During this process, these cells will exert forces on their surrounding tissue which will cause the tissue to deform. In order to calculate this deformation, we use the following balance of forces:

$$\nabla \cdot \underline{\underline{\sigma}} + \underline{\underline{g}} = 0, \quad (2.51)$$

In which $\underline{\underline{\sigma}}$ is the stress tensor and $\underline{\underline{g}}$ is the sum of all contractile forces on the tissue. Using this equation, we derive the displacement $\underline{\underline{u}}$ for each mesh point in each time step.

2.2.1. DEFORMATION

First, we derive the governing mechanical laws in three dimensions. Even though the considered domain is in two dimensions, we only apply this restriction in the last steps of the derivation. In

order to obtain a relationship between the stress tensor $\underline{\sigma}$ and the strain tensor $\underline{\varepsilon}$, we use Hooke's law:

$$E\varepsilon_{11} = \sigma_{11} - \nu\sigma_{22} - \nu\sigma_{33}, \quad (2.52a)$$

$$E\varepsilon_{22} = \sigma_{22} - \nu\sigma_{11} - \nu\sigma_{33}, \quad (2.52b)$$

$$E\varepsilon_{33} = \sigma_{33} - \nu\sigma_{11} - \nu\sigma_{22}, \quad (2.52c)$$

$$E\varepsilon_{12} = (1 + \nu)\sigma_{12}, \quad (2.52d)$$

$$E\varepsilon_{23} = (1 + \nu)\sigma_{23}, \quad (2.52e)$$

$$E\varepsilon_{13} = (1 + \nu)\sigma_{13}. \quad (2.52f)$$

In which E is the Young's modulus of the affected tissue and ν the Poisson ratio which are considered constant. We now rewrite (2.52) using matrix inversion so that the stress tensor is defined in terms of the strain tensor.

$$E \begin{bmatrix} \varepsilon_{11} \\ \varepsilon_{22} \\ \varepsilon_{33} \\ \varepsilon_{12} \\ \varepsilon_{23} \\ \varepsilon_{13} \end{bmatrix} = \begin{bmatrix} 1 & -\nu & -\nu & 0 & 0 & 0 \\ -\nu & 1 & -\nu & 0 & 0 & 0 \\ -\nu & -\nu & 1 & 0 & 0 & 0 \\ 0 & 0 & 0 & 1 + \nu & 0 & 0 \\ 0 & 0 & 0 & 0 & 1 + \nu & 0 \\ 0 & 0 & 0 & 0 & 0 & 1 + \nu \end{bmatrix} \begin{bmatrix} \sigma_{11} \\ \sigma_{22} \\ \sigma_{33} \\ \sigma_{12} \\ \sigma_{23} \\ \sigma_{13} \end{bmatrix}, \quad (2.53)$$

$$\begin{bmatrix} \sigma_{11} \\ \sigma_{22} \\ \sigma_{33} \\ \sigma_{12} \\ \sigma_{23} \\ \sigma_{13} \end{bmatrix} = \frac{E}{(1 + \nu)(1 - 2\nu)} \begin{bmatrix} 1 - \nu & \nu & \nu & 0 & 0 & 0 \\ \nu & 1 - \nu & \nu & 0 & 0 & 0 \\ \nu & \nu & 1 - \nu & 0 & 0 & 0 \\ 0 & 0 & 0 & 1 - 2\nu & 0 & 0 \\ 0 & 0 & 0 & 0 & 1 - 2\nu & 0 \\ 0 & 0 & 0 & 0 & 0 & 1 - 2\nu \end{bmatrix} \begin{bmatrix} \varepsilon_{11} \\ \varepsilon_{22} \\ \varepsilon_{33} \\ \varepsilon_{12} \\ \varepsilon_{23} \\ \varepsilon_{13} \end{bmatrix}. \quad (2.54)$$

The next step is to restrict this law to the two-dimensional case. All terms concerning the third dimension are therefore discarded. Equation (2.54) then simplifies to the following relationship:

$$\begin{bmatrix} \sigma_{11} \\ \sigma_{22} \\ \sigma_{12} \end{bmatrix} = \frac{E}{(1 + \nu)(1 - 2\nu)} \begin{bmatrix} 1 - \nu & \nu & 0 \\ \nu & 1 - \nu & 0 \\ 0 & 0 & 1 - 2\nu \end{bmatrix} \begin{bmatrix} \varepsilon_{11} \\ \varepsilon_{22} \\ \varepsilon_{12} \end{bmatrix}. \quad (2.55)$$

Since we aim at an equation concerning the displacement vector $\underline{u} = \begin{bmatrix} u \\ v \end{bmatrix}$, we use the relation between strain and displacement:

$$\underline{\varepsilon} = \frac{1}{2} (\nabla \underline{u} + (\nabla \underline{u})^T). \quad (2.56)$$

With the following definition and subscripted notation for differentiation,

$$\nabla \underline{u} = \begin{bmatrix} \frac{\partial}{\partial x} \\ \frac{\partial}{\partial y} \end{bmatrix} \begin{bmatrix} u & v \end{bmatrix} = \begin{bmatrix} u_x & v_x \\ u_y & v_y \end{bmatrix}, \quad (2.57)$$

this becomes:

$$\underline{\underline{\epsilon}} = \begin{bmatrix} u_x & \frac{1}{2}(v_x + u_y) \\ \frac{1}{2}(v_x + u_y) & v_y \end{bmatrix}. \quad (2.58)$$

Finally, by substituting (2.58) into (2.54), we can rewrite the stress tensor in terms of the displacement vector.

$$\underline{\underline{\sigma}} = \frac{E}{(1+\nu)(1-2\nu)} \begin{bmatrix} (1-\nu)u_x + \nu v_y & \frac{1}{2}(1-2\nu)(v_x + u_y) \\ \frac{1}{2}(1-2\nu)(v_x + u_y) & (1-\nu)v_y + \nu u_x \end{bmatrix}. \quad (2.59)$$

2.2.2. BOUNDARY CONDITIONS

As we can see in equation (2.51), the spatial dependency requires boundary conditions in order to find a unique solution for \underline{u} . To derive the correct boundary conditions, we consider the physical meaning of the four borders.

First, the northern boundary represents the surface of the skin. We assume no external forces exist on this side, therefore the surface should have a freedom of motion. Mathematically, this means that the following boundary condition is imposed:

$$\underline{\underline{\sigma}} \cdot \underline{n} = 0, \quad \text{on } \Gamma^N, \quad (2.60)$$

In which \underline{n} is the outward pointing normal vector on Γ^N . The remaining three borders represent the boundary towards undamaged tissue. A displacement here will cause an opposite force from this surrounding tissue. Mechanically speaking, this is analogous to applying springs on these boundaries with a certain spring constant κ . The final boundary conditions then become:

$$\underline{\underline{\sigma}} \cdot \underline{n} = -\kappa \underline{u}, \quad \text{on } \Gamma^E \cup \Gamma^W \cup \Gamma^S, \quad \kappa > 0. \quad (2.61)$$

2.2.3. WEAK FORMULATION

Let us consider the force balance equation as shown by equation (2.51):

$$\nabla \cdot \underline{\underline{\sigma}} = -\underline{g}. \quad (2.62)$$

We split this up into two separate equations for the elements of \underline{g} :

$$\nabla \cdot \begin{bmatrix} \sigma_{11} \\ \sigma_{12} \end{bmatrix} = -g_1, \quad (2.63)$$

$$\nabla \cdot \begin{bmatrix} \sigma_{12} \\ \sigma_{22} \end{bmatrix} = -g_2. \quad (2.64)$$

Let us start with the first equation. We multiply with a test function $\varphi \in \mathcal{H}^1(\Omega)$ and integrate over the entire domain Ω . We then use integration by parts and substitute equation (2.59) in order to get

an equation for the displacement $[u \ v]^T$.

$$\int_{\Omega_t} \nabla \cdot \begin{bmatrix} \sigma_{11} \\ \sigma_{21} \end{bmatrix} \varphi \, d\Omega_t = - \int_{\Omega_t} g_1 \varphi \, d\Omega_t \quad (2.65)$$

$$\int_{\Gamma} \underline{n} \cdot \begin{bmatrix} \sigma_{11} \\ \sigma_{21} \end{bmatrix} \varphi \, d\Gamma - \frac{E}{(1+\nu)(1-2\nu)} \int_{\Omega_t} \nabla \varphi \cdot \begin{bmatrix} (1-\nu)u_x + \nu v_y \\ (1-2\nu)\frac{1}{2}(v_x + u_y) \end{bmatrix} \, d\Omega_t = - \int_{\Omega_t} g_1 \varphi \, d\Omega_t. \quad (2.66)$$

Applying the boundary conditions yields:

$$- \int_{\Gamma \setminus \Gamma^N} s \rho_c u \varphi \, d\Gamma - \frac{E}{(1+\nu)(1-2\nu)} \int_{\Omega_t} \nabla \varphi \cdot \begin{bmatrix} (1-\nu)u_x + \nu v_y \\ (1-2\nu)\frac{1}{2}(v_x + u_y) \end{bmatrix} \, d\Omega_t = - \int_{\Omega_t} g_1 \varphi \, d\Omega_t \quad (2.67)$$

$$\begin{aligned} & \int_{\Gamma \setminus \Gamma^N} s \rho_c u \varphi \, d\Gamma + \\ & \frac{E}{(1+\nu)(1-2\nu)} \int_{\Omega_t} (1-\nu)u_x \varphi_x + (1-2\nu)\frac{1}{2}u_y \varphi_y + \nu v_y \varphi_x + (1-2\nu)\frac{1}{2}v_x \varphi_y \, d\Omega_t = \int_{\Omega_t} g_1 \varphi \, d\Omega_t. \end{aligned} \quad (2.68)$$

Analogous to this derivation, we find the weak form of the second equation. This results in the following:

$$\begin{aligned} & \int_{\Gamma \setminus \Gamma^N} s \rho_c v \varphi \, d\Gamma + \\ & \frac{E}{(1+\nu)(1-2\nu)} \int_{\Omega_t} (1-2\nu)\frac{1}{2}v_x \varphi_x + (1-\nu)v_y \varphi_y + (1-2\nu)\frac{1}{2}u_y \varphi_x + \nu u_x \varphi_y \, d\Omega_t = \int_{\Omega_t} g_2 \varphi \, d\Omega_t. \end{aligned} \quad (2.69)$$

2.2.4. CONTRACTILE FORCES

The remaining term in equation (2.51) is the force term \underline{g} . In this model, we are interested in the contractile forces exerted by the (myo)fibroblasts. These forces can be split up into two types. First of all, (myo)fibroblasts constantly pull on their direct surroundings and let go once they move on. Since these forces are not permanent, these are named temporary forces (\underline{F}_{temp}). On the other hand, myofibroblasts will form knots in the fiber bundles which exert a constant force on the surrounding tissue. These forces will be called plastic forces (\underline{F}_{pl}).

In this section we will consider a general domain Ω upon which the deformation is calculated. For simplicity, the boundary $\delta\Omega$ is suspended by a spring with stiffness constant $\kappa > 0$. Adding this to equation (2.51), we consider the following case:

$$\begin{cases} \nabla \cdot \underline{\sigma} + \underline{F}_{temp} + \underline{F}_{pl} = \underline{0} & \text{in } \Omega, \\ \underline{\sigma} \cdot \underline{n} + \kappa \underline{u} = \underline{0} & \text{on } \delta\Omega. \end{cases} \quad (2.70)$$

TEMPORARY FORCES

In order to formulate the temporary forces, it is important to consider what happens when a point force is added to the domain at coordinates (\hat{x}, \hat{y}) . Let this force act in direction $\underline{P} = [P_x \ P_y]^T$ with

magnitude $\|P\|$. The mechanical balance then reads as:

$$\begin{cases} \nabla \cdot \underline{\underline{\sigma}} + \underline{\underline{P}} \delta(\underline{\underline{x}} - \underline{\underline{\hat{x}}}) = \underline{\underline{0}} & \text{in } \Omega, \\ \underline{\underline{\sigma}} \cdot \underline{\underline{n}} + \kappa \underline{\underline{u}} = \underline{\underline{0}} & \text{on } \delta\Omega. \end{cases} \quad (2.71)$$

However, a (myo)fibroblast cannot be considered as a single point force since it does not exert a force in one specific direction. Rather, all of the surrounding tissue is pulled towards its center and therefore a different approach is required.

Let us consider a single (myo)fibroblast at coordinates $\underline{\underline{x}}_c$ within the domain. We will assume that the temporary forces are then exerted on a closed curve $\delta\Omega_c$ enclosing $\Omega_c \ni \underline{\underline{x}}_c$. We divide this curve $\delta\Omega_c$ into line-segments l_j with length Δl_j . Let P_0 be the force per unit of length, then at any point $(x_j, y_j) \in \delta\Omega_c$ on line-segment l_j , we get:

$$\begin{cases} \nabla \cdot \underline{\underline{\sigma}} + P_0 \underline{\underline{n}}(x_j, y_j) \delta(\underline{\underline{x}} - \underline{\underline{x}}_j) \Delta l_j = \underline{\underline{0}} & \text{in } \Omega, \\ \underline{\underline{\sigma}} \cdot \underline{\underline{n}} + \kappa \underline{\underline{u}} = \underline{\underline{0}} & \text{in } \delta\Omega. \end{cases} \quad (2.72)$$

With $\underline{\underline{n}}(x_j, y_j)$ the unit normal vector on $\delta\Omega_c$ at $\underline{\underline{x}}_j$ pointing into Ω_c . The total force is then given by summation over all line-segments:

$$\underline{\underline{F}}_{temp} = \sum_{j=1}^{n_l} P_0 \underline{\underline{n}}(x_j, y_j) \delta(\underline{\underline{x}} - \underline{\underline{x}}_j) \Delta l_j. \quad (2.73)$$

Since we use a finite element framework, we aim to find a weak form. This is achieved by multiplying by a test function $\varphi \in \mathcal{H}^1(\Omega)$ and integrating over Ω :

$$\begin{aligned} \int_{\Omega} \varphi \underline{\underline{F}}_{temp} d\Omega &= \int_{\Omega} \varphi \sum_{j=1}^{n_l} P_0 \underline{\underline{n}}(x_j, y_j) \delta(\underline{\underline{x}} - \underline{\underline{x}}_j) \Delta l_j d\Omega \\ &= P_0 \sum_{j=1}^{n_l} \int_{\Omega} \varphi \underline{\underline{n}}(x_j, y_j) \delta(\underline{\underline{x}} - \underline{\underline{x}}_j) d\Omega \Delta l_j \\ &= P_0 \sum_{j=1}^{n_l} \varphi(x_s, y_s) \underline{\underline{n}}(x_s, y_s) \Delta l_j. \end{aligned} \quad (2.74)$$

Note that if we let $n_l \rightarrow \infty$ and therewith $\Delta l_j \downarrow 0$, then the Riemann sum gives

$$\int_{\Omega} \varphi \underline{\underline{F}}_{temp} d\Omega = P_0 \int_{\delta\Omega_c} \varphi(x_s, y_s) \underline{\underline{n}}(x_s, y_s) d\Gamma(x_s, y_s). \quad (2.75)$$

Substituting this into 2.72, we consider the following boundary value problem:

$$\begin{cases} \nabla \cdot \underline{\underline{\sigma}} + \int_{\delta\Omega_c} P_0 \underline{\underline{n}}(x_s, y_s) \delta(\underline{\underline{x}} - \underline{\underline{x}}_s) d\Gamma(x_s, y_s) = \underline{\underline{0}} & \text{in } \Omega, \\ \underline{\underline{\sigma}} \cdot \underline{\underline{n}} + \kappa \underline{\underline{u}} = \underline{\underline{0}} & \text{in } \delta\Omega. \end{cases} \quad (2.76)$$

What remains is the choice of curve surrounding the fibroblast. Initially, a circle would seem most appropriate since the cells are modeled as discrete discs moving through the mesh. Using a radius of r_c , (2.74) can be rewritten:

$$\int_{\Omega} \varphi \underline{F}_{temp} d\Omega = -P_0 r_c \int_0^{2\pi} \varphi \left(\underline{x}_f + \begin{bmatrix} \cos(\theta) \\ \sin(\theta) \end{bmatrix} \right) \begin{bmatrix} \cos(\theta) \\ \sin(\theta) \end{bmatrix} d\theta. \quad (2.77)$$

Since the cells are not necessarily contained in a single element, numerous geometric possibilities can arise. Considering this, the integral (2.77) becomes too complex to evaluate in each time step.

A simple solution to this problem is to fall back on equation (2.73) and consider the curve, upon which the temporary forces are exerted, as a square. In doing so, we can use the four midpoints of its sides.

$$\underline{F}_{temp} = \sum_{j=1}^4 P_0 \underline{n}(x_j, y_j) \delta(\underline{x} - \underline{x}_j) \Delta l_j. \quad (2.78)$$

By letting the square have sides of length $2r_s$, we can calculate r_s such that the area of influence is the same as in the circular case.

$$4r_s^2 = \pi r_c^2 \Rightarrow r_s = \frac{\sqrt{\pi}}{2} r_c. \quad (2.79)$$

We now define the four midpoints as follows:

$$\begin{aligned} \underline{x}_c^E &= \begin{bmatrix} x_c + r_s \\ y_c \end{bmatrix}, & \underline{x}_c^W &= \begin{bmatrix} x_c - r_s \\ y_c \end{bmatrix}, \\ \underline{x}_c^N &= \begin{bmatrix} x_c \\ y_c + r_s \end{bmatrix}, & \underline{x}_c^S &= \begin{bmatrix} x_c \\ y_c - r_s \end{bmatrix}. \end{aligned}$$

Using this definition, equation (2.78) is rewritten as follows:

$$\begin{aligned} \underline{F}_{temp} &= 2r_s P_0 \left(\delta(\underline{x} - \underline{x}_c^E) \begin{bmatrix} -1 \\ 0 \end{bmatrix} + \delta(\underline{x} - \underline{x}_c^W) \begin{bmatrix} 1 \\ 0 \end{bmatrix} \right. \\ &\quad \left. + \delta(\underline{x} - \underline{x}_c^N) \begin{bmatrix} 0 \\ -1 \end{bmatrix} + \delta(\underline{x} - \underline{x}_c^S) \begin{bmatrix} 0 \\ 1 \end{bmatrix} \right) \\ &= -2r_s P_0 \begin{bmatrix} \delta(\underline{x} - \underline{x}_c^E) - \delta(\underline{x} - \underline{x}_c^W) \\ \delta(\underline{x} - \underline{x}_c^N) - \delta(\underline{x} - \underline{x}_c^S) \end{bmatrix}. \end{aligned} \quad (2.80)$$

As the collagen density increases, more bundles are available to exert forces on. Therefore, a factor is added to (2.80) which will increase the temporary forces when the collagen density is higher. The final formulation now becomes:

$$\underline{F}_{temp} = -2r_s \rho_c P_0 \begin{bmatrix} \delta(\underline{x} - \underline{x}_c^E) - \delta(\underline{x} - \underline{x}_c^W) \\ \delta(\underline{x} - \underline{x}_c^N) - \delta(\underline{x} - \underline{x}_c^S) \end{bmatrix}. \quad (2.81)$$

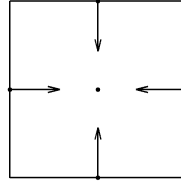


Figure 2.8: Temporary forces on a square curve around the center.

Here, we introduce the first difference between myofibroblasts and fibroblasts. Both species behave in a similar manner but differ in the size of the contractile forces which they exert. Therefore, the formulation of these temporary forces is the same for both cell types, but the value of P_0 is higher for myofibroblasts than for regular fibroblasts:

$$P_0^k = \begin{cases} P_0^f, & \text{if cell } k \text{ is a fibroblast} \\ P_0^m, & \text{if cell } k \text{ is a myofibroblast} \end{cases}, \quad \text{with } P_0^f \leq P_0^m. \quad (2.82)$$

Now, the weak form can be found by using the formulation with Dirac delta functions to our advantage. This derivation is done as follows:

$$\int_{\Omega} \varphi \underline{F}_{temp} d\Omega = \int_{\Omega} -2r_s \rho_c P_0 \begin{bmatrix} \delta(\underline{x} - \underline{x}_c^E) - \delta(\underline{x} - \underline{x}_c^W) \\ \delta(\underline{x} - \underline{x}_c^N) - \delta(\underline{x} - \underline{x}_c^S) \end{bmatrix} \varphi d\Omega \quad (2.83)$$

$$= -2r_s P_0 \begin{bmatrix} \rho_c(\underline{x}_c^E) \varphi(\underline{x}_c^E) - \rho_c(\underline{x}_c^W) \varphi(\underline{x}_c^W) \\ \rho_c(\underline{x}_c^N) \varphi(\underline{x}_c^N) - \rho_c(\underline{x}_c^S) \varphi(\underline{x}_c^S) \end{bmatrix}. \quad (2.84)$$

PLASTIC FORCES

Next, we consider the incorporation of plastic forces in which myofibroblasts form so-called knots in the fiber bundles. These forces differ from the temporary forces since they remain permanently in an element, even after a cell has left or died. An artificial timer τ is therefore introduced for each element in order to keep track of the progress in the process of knot creation. This timer is incremented by $\Delta\tau$ whenever a myofibroblast is present. The value of $\Delta\tau$ in an element e is determined by the size of the area that the myofibroblast overlaps with the area of the element.

$$\Delta\tau_e = \frac{\mathcal{A}(\Omega_e \cap \Omega_c)}{\mathcal{A}(\Omega_e)} \Delta t. \quad (2.85)$$

In which $\mathcal{A}(\Omega)$ denotes the area of Ω , Ω_c is the disk representing a myofibroblast and Ω_e is element e in the finite element mesh. Unfortunately, the value of $\mathcal{A}(\Omega_e \cap \Omega_c)$ becomes difficult to determine because of the numerous different geometric possibilities which arise when the cells move through the mesh.

In order to overcome these difficulties, we once again consider the cells as five discrete points instead of disks. We then consider these five points to have an equal area for which they are responsible. In Figure 2.9, an illustration is given describing how this can be considered.

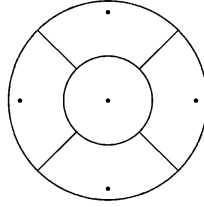


Figure 2.9: Dividing the circular area of influence into five equal pieces. The five points are used to approximate the overlapping area between the myofibroblast and an element.

By calculating the number of points (n_{mp}) in an element, a rough approximation can be made of the overlapping area between the cell and the element. Using $\frac{1}{2}|\Delta_e|$ as the area of element e , we rewrite (2.85) as follows:

$$\Delta\tau \approx \frac{n_{mp}}{5} 4r_s^2 \cdot \frac{1}{\frac{1}{2}|\Delta_e|} \Delta t. \quad (2.86)$$

Analogous to the temporary forces, forces are only exerted on the surrounding tissue when collagen bundles are present. In this formulation, this is implemented in the value of $\Delta\tau$. With the incorporation of the average collagen density in the element (ρ_{ce}), we obtain:

$$\Delta\tau_e = \rho_{ce} \frac{n_{mp}}{5} 4r_s^2 \cdot \frac{2}{|\Delta_e|} \Delta t. \quad (2.87)$$

As mentioned before, the value of τ determines the size of the plastic forces in the corresponding element. The magnitude of the force P is therefore a function of τ . The next step is to formulate the function $P(\tau)$. First of all, it should converge to a maximum P_{max} with a certain rate α_τ as τ is increased. Secondly, if τ is zero, the value of P should also be zero. Both of these conditions combined describe the following initial value problem.

$$\begin{cases} \frac{\partial P}{\partial \tau} = \alpha_\tau (P_{max} - P), \\ P(0) = 0. \end{cases} \quad (2.88)$$

By solving initial value problem (2.88), we obtain:

$$P(\tau) = P_{max} (1 - e^{-\alpha_\tau \tau}). \quad (2.89)$$

Since each element is triangular, we can split up its boundaries into the three edges and their corresponding midpoints. Once again, we use the form described in (2.73) to formulate the plastic

forces.

$$\underline{F}_{pl}^e = \sum_{j=1}^3 P(\tau_e) \underline{n}(\underline{x}_j^e) \delta(\underline{x} - \underline{x}_j^e) \Delta l_j, \quad (2.90)$$

In which \underline{x}_j^e is a midpoint on the edge of the element and $\underline{n}(\underline{x}_j^e)$ represents the unit normal vector pointing into the element e . Figure 2.10 gives a representation of the three directions in an element in which the plastic forces are exerted.

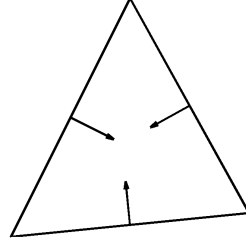


Figure 2.10: The three directions of the plastic forces for an element.

Finally, we derive the weak form by multiplying by a test function $\varphi \in \mathcal{H}^1(\Omega)$ and integrating over Ω .

$$\int_{\Omega} \varphi \underline{F}_{pl}^e d\Omega = \int_{\Omega} \varphi \sum_{j=1}^3 P(\tau_e) \underline{n}(\underline{x}_j^e) \delta(\underline{x} - \underline{x}_j^e) \Delta l_j d\Omega \quad (2.91)$$

$$= \sum_{j=1}^3 P(\tau_e) \underline{n}(\underline{x}_j^e) \varphi(\underline{x}_j^e) \Delta l_j \quad (2.92)$$

The size and direction of the plastic forces are now defined. In conclusion of this formulation, Figure 2.11 gives a representation of the possible directions in a predefined mesh.

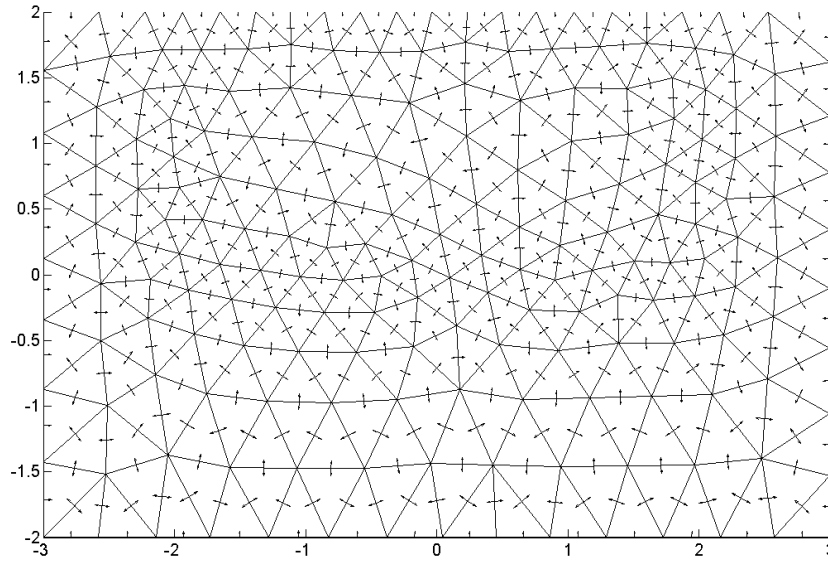


Figure 2.11: Directions of plastic forces in all elements. By increasing the artificial time τ for different elements, the corresponding forces are increased.

2.2.5. INCORPORATION OF A MOVING MESH

With the addition of contraction, the domain is altered in each time step. By calculating the displacement from the initial grid \underline{u}_p on each mesh point \underline{x}_p , we find the new position for these points:

$$\underline{x}_p^{i+1} = \underline{x}_p^0 + \underline{u}_p^{i+1}. \quad (2.93)$$

Since we also have

$$\underline{x}_p^i = \underline{x}_p^0 + \underline{u}_p^i, \quad (2.94)$$

we get

$$\underline{x}_p^{i+1} = \underline{x}_p^i + \underline{u}_p^{i+1} - \underline{u}_p^i. \quad (2.95)$$

The effect that a dynamic domain has on the behavior of the different mediators needs to be implemented as well. We will show the influence for both the continuum and the discrete entities.

CONTINUUM ENTITIES

If we add contraction to the model, then the moving tissue will produce convective fluxes on the different concentrations. For example, as an area shrinks in size due to contractile forces, the concentrations of cytokines will rise. To show the effect of this dynamic domain, we use a general formulation of the affected differential equations:

$$\frac{\partial \phi}{\partial t} = f(\phi, x, t). \quad (2.96)$$

We now implement the dynamics of a moving domain into the differential equations by adding the term $\nabla \cdot (\phi \underline{v})$ to the left-hand side in which \underline{v} is the vector field describing the velocity inside the domain.

$$\frac{\partial \phi}{\partial t} + \nabla \cdot (\phi \underline{v}) = f(\phi, x, t). \quad (2.97)$$

We rewrite equation (2.97) using the total, or material derivative $\frac{D}{Dt}$

$$\frac{\partial \phi}{\partial t} + \underline{v} \cdot \nabla \phi + \phi(\nabla \cdot \underline{v}) = f(\phi, x, t), \quad (2.98)$$

$$\frac{D\phi}{Dt} + \phi(\nabla \cdot \underline{v}) = f(\phi, x, t). \quad (2.99)$$

Since we use a finite element method to solve this equation, we construct the weak formulation. Therefore, we multiply both sides of the equation by a test function $\varphi \in \mathcal{H}^1(\Omega)$ and integrate over the entire domain. Since the domain is no longer stationary, it will be denoted by Ω_t .

$$\int_{\Omega_t} \frac{D\phi}{Dt} \varphi + \phi(\nabla \cdot \underline{v}) \varphi \, d\Omega_t = \int_{\Omega_t} f(\phi, x, t) \varphi \, d\Omega_t, \quad (2.100)$$

$$\int_{\Omega_t} \frac{D(\phi\varphi)}{Dt} - \phi \frac{D\varphi}{Dt} + \phi\varphi(\nabla \cdot \underline{v}) \, d\Omega_t = \int_{\Omega_t} f(\phi, x, t) \varphi \, d\Omega_t. \quad (2.101)$$

At this stage, we use Reynolds Transport Theorem (Wesseling, 2001) to simplify the left-hand side.

$$\frac{D}{Dt} \int_{\Omega_t} \phi\varphi \, d\Omega_t - \int_{\Omega_t} \phi \frac{D\varphi}{Dt} \, d\Omega_t = \int_{\Omega_t} f(\phi, x, t) \varphi \, d\Omega_t. \quad (2.102)$$

Finally, we consider the term $\frac{D\varphi}{Dt}$. By choosing φ as a linear basis function on the triangular elements and incorporating a moving mesh, we may use

$$\frac{D\varphi}{Dt} = 0, \quad (2.103)$$

as proved by Dziuk and Elliott (2007). This simplifies (2.102) to the following:

$$\frac{D}{Dt} \int_{\Omega_t} \phi\varphi \, d\Omega_t = \int_{\Omega_t} f(\phi, x, t) \varphi \, d\Omega_t. \quad (2.104)$$

Note that the right-hand side remains unchanged except for the added time dependency of the domain Ω .

DISCRETE MEDIATORS

Due to the movement of the tissue, the movement of cells through the mesh is affected as well. Apart from the different influences on cell movement explained in chapters 2.1.4 and 2.1.6, a new term needs to be added to account for this movement of the tissue. The cells need to be carried in each time step towards the new topology of the domain. Since the displacement vectors for the current and next time steps are already calculated beforehand, we use these to our advantage. By interpolating the values of \underline{u}_p , we obtain the displacement at the cell positions \underline{u}_c . Using equation

(2.95), the update as described in equation (2.25) is then altered to:

$$\underline{x}_c^{i+1} = \underline{x}_c^i + d\underline{x}_c + \underline{u}_c^{i+1} - \underline{u}_c^i. \quad (2.105)$$

The influence from contact forces between cells are incorporated after this update.

3

NUMERICAL IMPLEMENTATION

Having formulated the various components and governing equations in the model, its numerical implementation presents its own challenges. In order to give an insight to these challenges, a few components have been selected and will be elaborated upon in this chapter. First, we consider the domain of computation and compute the triangular mesh upon which the continuum entities are calculated. Second, the manner in which the initial conditions for both the discrete and continuum entities are implemented is explained. Third, we describe the finite element method used to calculate the values associated with the different continuum entities. Third, the interpolation scheme is presented which is necessary in order to calculate the value of the continuum entities at a cell's location. Finally, we give an overview of the entire numerical integration scheme.

3.1. DOMAIN

The domain of computation consists of a cross-section of the upper part of the skin, such that the top represents the skin boundary. Since the wounds considered in this model are inflicted by an external source, a region at the top of the domain will serve as the wound space. The rest will be considered undamaged tissue as shown in Figure 3.1. The size of the domain is $1200 \mu\text{m}$ in width and $1600 \mu\text{m}$ in height. In order to non-dimensionalize the domain, it is scaled by a factor of $400 \mu\text{m}$ in each direction resulting in a domain of 3×4 . The same is done for the wound space which was originally $400 \mu\text{m} \times 800 \mu\text{m}$ and therefore becomes 1×2 .

As shown by Cumming et al. (2010), this domain is suitable for modeling an incision-like wound with a depth larger than its width. Since wound contraction is our main point of interest, we aim to build a model which can form a basis for modeling wounds with a large area. Therefore, the first adjustment to the model will be to consider a wound with different proportions such that its width is larger than its depth. The new dimensions for the entire domain then become 6×4 and the wound space becomes 4×2 .

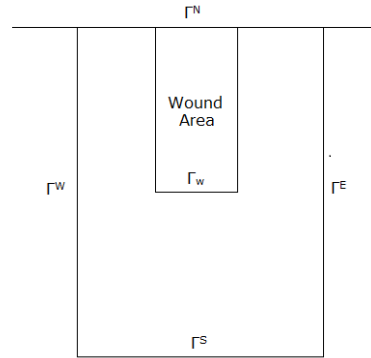


Figure 3.1: The original domain of computation used in Cumming et al. (2010) showing the wound space at the top surrounded by undamaged tissue and the four boundaries.

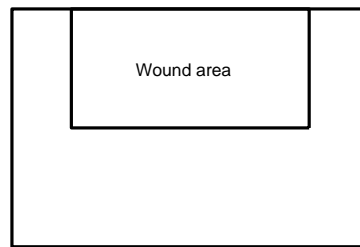


Figure 3.2: Adjusted domain since we consider wounds with different proportions. The width of the wound is now larger than its depth.

Finally, a mesh is created for the entire domain. With the addition of contraction, the domain will be deformed in such ways that a rectangular mesh is undesirable. A triangular mesh is therefore created which is more adaptable to such deformations. Furthermore, the mesh will have a higher density in the more interesting regions of the domain, namely the boundary between the wound area and undamaged tissue and the top boundary of the wound space. Figure 3.3 shows an example of such a mesh.

3.2. INITIAL CONDITIONS

As we have seen in Chapter 2.1, the initial values of the different continuum species are known beforehand. These values are therefore implemented at $t = 0$. However, the initial conditions for the fibroblast and myofibroblast populations is not yet well-defined.

The initial distribution of (myo)fibroblasts is assumed to be uniform throughout the undamaged tissue. Let us assume there are n_f^0 initial cells in the domain. We then set their coordinates according to the procedure described in Algorithm 3.1.

Afterwards, the labels are assigned to each cell to define whether it is a fibroblast or a myofibroblast. This label is only consulted in the component of the model which calculates the contraction.

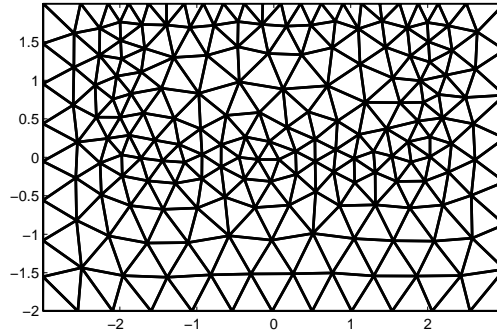


Figure 3.3: Triangular mesh on the domain of computation. Note that the mesh is denser near the boundary of the wound space and the top boundary.

Algorithm 3.1 Iterative scheme to establish a uniform distribution of (myo)fibroblasts in undamaged tissue

Calculate initial cell positions by taking n_f^0 samples from a uniform distribution on Ω .

repeat

Define $\mathcal{L} = \emptyset$, the empty set.

Find cells in the wound space Ω_w and add the corresponding indices to the set \mathcal{L} .

Find overlapping cells in Ω and add one index from each overlap to the set \mathcal{L} .

Calculate new cell positions for cells with indices in \mathcal{L} by taking samples from a uniform distribution.

until $\mathcal{L} = \emptyset$

3.3. FINITE ELEMENT METHOD

We now consider the continuum equations that are governed by differential equations. These will be solved using a finite element method analogous to the methods described in Van Kan et al. (2008). We consider fibrin decay in order to show the effects of a moving grid and the challenges corresponding to nonlinear dependencies. Furthermore, we consider collagen synthesis which is an example of the interaction between discrete entities and the triangular mesh.

3.3.1. FIBRIN DECAY

Let us start by considering the process of fibrin decay and the governing equation for the tPA concentration. For notational simplicity and to avoid ambiguity with the time variable t , we denote the tPA concentration with ϕ .

$$\frac{\partial \phi}{\partial t} + \nabla \cdot (\phi \underline{v}) = \nabla \cdot ((D_{max}(1 - \rho_f) + \rho_f D_{min}) \nabla \phi) + T. \quad (3.1)$$

We now multiply both sides of the equation with a test function $\varphi \in \mathcal{H}^1(\Omega_t)$ and integrate over the entire domain in order to create a weak form. For the left hand side, we use the derivation explained in Section 2.2.5:

$$\frac{D}{Dt} \int_{\Omega_t} \phi \varphi \, d\Omega_t = \int_{\Omega_t} \nabla \cdot (D_{max} + \rho_f(D_{min} - D_{max})\nabla\phi) \varphi + T\varphi \, d\Omega_t, \quad (3.2)$$

$$\frac{D}{Dt} \int_{\Omega_t} \phi \varphi \, d\Omega_t = \int_{\Omega_t} D_{max}(\nabla \cdot \nabla\phi) \varphi + (D_{min} - D_{max})\nabla \cdot (\rho_f \nabla\phi) \varphi + T\varphi \, d\Omega_t. \quad (3.3)$$

The next step is to use integration by parts:

$$\begin{aligned} \frac{D}{Dt} \int_{\Omega_t} \phi \varphi \, d\Omega_t &= D_{max} \int_{\Omega_t} \nabla \cdot (\nabla\phi \varphi) - \nabla\phi \cdot \nabla\varphi \, d\Omega_t \\ &\quad + (D_{min} - D_{max}) \int_{\Omega_t} \nabla \cdot (\rho_f \nabla\phi \varphi) - \rho_f \nabla\phi \cdot \nabla\varphi \, d\Omega_t + \int_{\Omega_t} T\varphi \, d\Omega_t \end{aligned} \quad (3.4)$$

$$\begin{aligned} &= D_{max} \left[\int_{\Gamma_t} \underline{n} \cdot (\nabla\phi \varphi) \, d\Gamma_t - \int_{\Omega_t} \nabla\phi \cdot \nabla\varphi \, d\Omega_t \right] \\ &\quad + (D_{min} - D_{max}) \left[\int_{\Gamma_t} \underline{n} \cdot (\rho_f \nabla\phi \varphi) \, d\Gamma_t - \int_{\Omega_t} \rho_f \nabla\phi \cdot \nabla\varphi \, d\Omega_t \right] + \int_{\Omega_t} T\varphi \, d\Omega_t. \end{aligned} \quad (3.5)$$

We are now ready to apply the boundary conditions for ϕ . As shown in Chapter 2.1, these boundary conditions are as follows:

$$\begin{cases} \underline{n} \cdot \nabla\phi = 0, & \text{on } \Gamma_t^N, \\ \underline{n} \cdot \nabla\phi = -\kappa\phi, & \text{on } \Gamma_t \setminus \Gamma_t^N, \quad \kappa > 0. \end{cases} \quad (3.6)$$

Applying these to equation (3.5), we derive:

$$\begin{aligned} \frac{D}{Dt} \int_{\Omega_t} \phi \varphi \, d\Omega_t &= D_{max} \left[\int_{\Gamma_t \setminus \Gamma_t^N} -\phi \varphi \, d\Gamma_t - \int_{\Omega_t} \nabla\phi \cdot \nabla\varphi \, d\Omega_t \right] \\ &\quad + (D_{min} - D_{max}) \left[\int_{\Gamma_t \setminus \Gamma_t^N} -\rho_f \phi \varphi \, d\Gamma_t - \int_{\Omega_t} \rho_f \nabla\phi \cdot \nabla\varphi \, d\Omega_t \right] + \int_{\Omega_t} T\varphi \, d\Omega_t. \end{aligned} \quad (3.7)$$

We approximate ϕ using linear elements as follows:

$$\phi(x, t) \approx \sum_{j=1}^{n_p} a_j(t) \varphi_j(x, t). \quad (3.8)$$

In which the time dependence of φ results from the movement of the mesh. Furthermore, we choose our test function to be φ_i with $i \in \{1 \dots n_p\}$ and substitute (3.8) into the left hand side of (3.7). Let us consider the result at time $t = t^n$:

$$\frac{D}{Dt} \int_{\Omega_t} \phi \varphi_i \, d\Omega_t \approx \frac{1}{\Delta t} \left[\sum_{j=1}^{n_p} a_j^{n+1} \int_{\Omega_t^{n+1}} \varphi_j^{n+1} \varphi_i^{n+1} \, d\Omega_t^{n+1} - \sum_{j=1}^{n_p} a_j^n \int_{\Omega_t^n} \varphi_j^n \varphi_i^n \, d\Omega_t^n \right] \quad (3.9)$$

The same is done for the terms on the right hand side of (3.7).

$$\int_{\Gamma_t \setminus \Gamma_t^N} -\phi \varphi_i d\Gamma_t - \int_{\Omega_t} \nabla \phi \cdot \nabla \varphi_i d\Omega_t \approx - \left[\int_{\Gamma_t \setminus \Gamma_t^N} \sum_{j=1}^{n_p} a_j \varphi_j \varphi_i d\Gamma_t + \int_{\Omega_t} \nabla \left(\sum_{j=1}^{n_p} a_j \varphi_j \right) \cdot \nabla \varphi_i d\Omega_t \right] \quad (3.10)$$

$$= - \sum_{j=1}^{n_p} a_j \left[\int_{\Gamma_t \setminus \Gamma_t^N} \varphi_j \varphi_i d\Gamma_t + \int_{\Omega_t} \nabla \varphi_j \cdot \nabla \varphi_i d\Omega_t \right] \quad (3.11)$$

Further we approximate ρ_f

$$\rho_f \approx \sum_{k=1}^{n_p} b_k \varphi_k, \quad (3.12)$$

and obtain the approximation for the remaining terms:

$$\begin{aligned} \int_{\Gamma_t \setminus \Gamma_t^N} -\rho_f \phi \varphi_i d\Gamma_t - \int_{\Omega_t} \rho_f \nabla \phi \cdot \nabla \varphi_i d\Omega_t &\approx - \int_{\Gamma_t \setminus \Gamma_t^N} \left(\sum_{k=1}^{n_p} b_k \varphi_k \right) \sum_{j=1}^{n_p} a_j \varphi_j \varphi_i d\Gamma_t \\ &\quad - \int_{\Omega_t} \left(\sum_{k=1}^{n_p} b_k \varphi_k \right) \nabla \left(\sum_{j=1}^{n_p} a_j \varphi_j \right) \cdot \nabla \varphi_i d\Omega_t \end{aligned} \quad (3.13)$$

$$= - \sum_{j=1}^{n_p} a_j \left[\sum_{k=1}^{n_p} b_k \int_{\Gamma_t \setminus \Gamma_t^N} \varphi_k \varphi_j \varphi_i d\Gamma_t + \sum_{k=1}^{n_p} b_k \int_{\Omega_t} \varphi_k \nabla \varphi_j \cdot \nabla \varphi_i d\Omega_t \right] \quad (3.14)$$

By evaluating the different integrals in (3.9), (3.11), and (3.14) for all different values of i , the different element vectors and matrices are created. We combine these into matrices S , $F(\underline{b})$, and vector \underline{T} in order to rewrite the problem to the following:

$$\frac{D}{Dt} (M\underline{a}) = -D_{max} S \underline{a} - (D_{min} - D_{max}) F(\underline{b}) \underline{a} + \underline{T}. \quad (3.15)$$

Where

$$M_{ij} = \int_{\Omega_t} \varphi_j \varphi_i d\Omega_t, \quad (3.16)$$

$$S_{ij} = \int_{\Gamma_t \setminus \Gamma_t^N} \varphi_j \varphi_i d\Gamma_t + \int_{\Omega_t} \nabla \varphi_j \cdot \nabla \varphi_i d\Omega_t, \quad (3.17)$$

$$F_{ij}(\underline{b}) = \sum_{k=1}^{n_p} b_k \int_{\Gamma_t \setminus \Gamma_t^N} \varphi_k \varphi_j \varphi_i d\Gamma_t + \sum_{k=1}^{n_p} b_k \int_{\Omega_t} \varphi_k \nabla \varphi_j \cdot \nabla \varphi_i d\Omega_t, \quad (3.18)$$

$$T_i = \int_{\Omega_t} T \varphi_i d\Omega_t. \quad (3.19)$$

Using an Euler Backward scheme, we obtain:

$$\frac{1}{\Delta t} [M^{n+1} \underline{a}^{n+1} - M^n \underline{a}^n] = -D_{max} S^{n+1} \underline{a}^{n+1} - (D_{min} - D_{max}) F^{n+1}(\underline{b}^{n+1}) \underline{a}^{n+1} + \underline{T}^{n+1} \quad (3.20)$$

Note that the matrix F^{n+1} depends on the value of \underline{b}^{n+1} which represents the fibrin density. The equation for the fibrin density as described by (2.1) is an ordinary differential equation for which we

are able to find the solution:

$$\frac{\partial \rho_f}{\partial t} = -r_p \phi_t \rho_f \quad (3.21)$$

$$\rho_f = \rho_f^0 \exp\left(-r_p \int_0^t \phi_t dt\right) \quad (3.22)$$

Combining equations (3.8), (3.12), and (3.22), we formulate the approximation element-wisely with $j \in \{1, 2, \dots, n_p\}$:

$$b_j^n = b_j^0 \exp\left(-r_p \Delta t \sum_{i=1}^n \frac{a_j^{i-1} + a_j^i}{2}\right) \quad (3.23)$$

$$b_j^{n+1} = b_j^0 \exp\left(-r_p \Delta t \sum_{i=1}^n \frac{a_j^{i-1} + a_j^i}{2} - r_p \Delta t \frac{a_j^n + a_j^{n+1}}{2}\right) \quad (3.24)$$

$$b_j^{n+1} = b_j^n \exp\left(-r_p \Delta t \frac{a_j^n + a_j^{n+1}}{2}\right). \quad (3.25)$$

This implementation finds the solution for a stationary grid. However, due to the added dynamics of the domain, equation (3.21) becomes:

$$\frac{\partial \rho_f}{\partial t} + \nabla \cdot (\rho_f \underline{v}) = -r_p \phi_t \rho_f \quad (3.26)$$

Finding the solution to this equation is not straightforward which shows that the addition of a moving grid can complicate even the simple equations. In this case, we derive the weak form:

$$\frac{D}{Dt} \int_{\Omega_t} \rho_f \varphi \, d\Omega_t = -r_p \int_{\Omega_t} \phi_t \rho_f \varphi \, d\Omega_t \quad (3.27)$$

We once again approximate ρ_f by $\sum_{k=1}^{n_p} b_k \varphi_k$ and choose the test function φ_i . Analogous to the previous derivation, we obtain the following equation for a certain matrix R dependent of \underline{a} :

$$\frac{1}{\Delta t} [M^{n+1} \underline{b}^{n+1} - M^n \underline{b}^n] = -r_p R^{n+1} (\underline{a}^{n+1}) \underline{b}^{n+1} \quad (3.28)$$

Finally, due to the nonlinear dependencies between \underline{a} and \underline{b} , the values will be calculated using a Picard iterative scheme. For notational simplicity, we rewrite equation (3.20) to the following:

$$[M^{n+1} + \Delta t D_{max} S^{n+1} + \Delta t (D_{min} - D_{max}) F^{n+1} (\underline{b}^{n+1})] \underline{a}^{n+1} = M^n \underline{a}^n + \Delta t \underline{T} \quad (3.29)$$

$$A(\underline{b}^{n+1}) \underline{a}^{n+1} = M^n \underline{a}^n + \Delta t \underline{T}. \quad (3.30)$$

Equation (3.28) is rewritten to a simpler formulation as well:

$$[M^{n+1} + \Delta t r_p R^{n+1} (\underline{a}^{n+1})] \underline{b}^{n+1} = M^n \underline{b}^n \quad (3.31)$$

$$B(\underline{a}^{n+1}) \underline{b}^{n+1} = M^n \underline{b}^n. \quad (3.32)$$

The final step is to formulate the Picard iterative scheme which is defined in algorithm 3.2. In this algorithm, k represents the iterate and $\varepsilon > 0$ is a predefined constant.

Algorithm 3.2 Iterative Picard scheme for tPA and Fibrin concentrations

The initial guess is the previous iterate: $\underline{b}_0^{n+1} = \underline{b}^n$.

$k \leftarrow 0$

repeat

Solve for $\underline{a}_{k+1}^{n+1}$

$$A(\underline{b}_k^{n+1}) \underline{a}_{k+1}^{n+1} = M^n \underline{a}^n + \Delta t \underline{T}. \quad (3.33)$$

Solve for $\underline{b}_{k+1}^{n+1}$

$$B(\underline{a}_{k+1}^{n+1}) \underline{b}_{k+1}^{n+1} = M^n \underline{b}^n. \quad (3.34)$$

Calculate the residual

$$r = M^n \underline{a}^n + \Delta t \underline{T} - A(\underline{b}_{k+1}^{n+1}) \underline{a}_{k+1}^{n+1}, \quad (3.35)$$

$k \leftarrow k + 1$.

until $\|r\| \leq \varepsilon \|\underline{a}_k^{n+1}\|$

3.3.2. COLLAGEN SYNTHESIS

Let us consider the synthesis of collagen which is described in equation (2.34). The synthesis depends on the collagen density ρ_c which equals the trace of $\Psi = \begin{bmatrix} \Psi_{xx} & \Psi_{xy} \\ \Psi_{xy} & \Psi_{yy} \end{bmatrix}$. Let us consider equation (2.34) in which we substitute this definition.

$$\frac{\partial \Psi_{xx}}{\partial t} = (1 - \rho_f - \rho_c) \sum_{i_c=1}^{n_f} (k_2 n_{i_c} + k_1 (1 - n_{i_c})) g_{i_c,x}^2 \mathbb{1}_c^i(\underline{x}), \quad (3.36)$$

$$\frac{\partial \Psi_{yy}}{\partial t} = (1 - \rho_f - \Psi_{xx} - \Psi_{yy}) \sum_{i_c=1}^{n_f} (k_2 n_{i_c} + k_1 (1 - n_{i_c})) g_{i_c,x}^2 \mathbb{1}_c^i(\underline{x}). \quad (3.37)$$

Due to its dependency on Ψ_{yy} , the equations for Ψ_{yy} and Ψ_{xx} are coupled and need to be evaluated as such. Therefore, we combine the equations for Ψ_{xx} and Ψ_{yy} in a single equation:

$$\frac{\partial}{\partial t} \begin{bmatrix} \Psi_{xx} \\ \Psi_{yy} \end{bmatrix} = \left(\sum_{i_c=1}^{n_f} (k_2 n_{i_c} + k_1 (1 - n_{i_c})) \begin{bmatrix} g_{i_c,x}^2 & 0 \\ 0 & g_{i_c,y}^2 \end{bmatrix} \mathbb{1}_c^i(\underline{x}) \right) \left(\begin{bmatrix} 1 - \rho_f \\ 1 - \rho_f \end{bmatrix} - \begin{bmatrix} 1 & 1 \\ 1 & 1 \end{bmatrix} \begin{bmatrix} \Psi_{xx} \\ \Psi_{yy} \end{bmatrix} \right). \quad (3.38)$$

In order to derive its weak form, we multiply by a test function φ and integrate over Ω_t . This can be done for both equations separately:

$$\int_{\Omega_t} \frac{\partial \Psi_{xx}}{\partial t} \varphi \, d\Omega_t = \int_{\Omega_t} (1 - \rho_f - \Psi_{xx} - \Psi_{yy}) \sum_{i_c=1}^{n_f} (k_2 n_{i_c} + k_1 (1 - n_{i_c})) g_{i_c,x}^2 \mathbb{1}_c^i(\underline{x}) \varphi \, d\Omega_t \quad (3.39)$$

$$\frac{D}{Dt} \int_{\Omega_t} \Psi_{xx} \varphi \, d\Omega_t = \sum_{i_c=1}^{n_f} \int_{\Omega_c^{i_c}} (1 - \rho_f - \Psi_{xx} - \Psi_{yy}) (k_2 n_{i_c} + k_1 (1 - n_{i_c})) g_{i_c,x}^2 \varphi \, d\Omega_c. \quad (3.40)$$

We now approximate Ψ_{xx} , Ψ_{yy} and ρ_f using linear elements and choose the test function φ_i with $i \in \{1 \dots n_p\}$. The right hand side then becomes:

$$\begin{aligned} & \sum_{i_c=1}^{n_f} \int_{\Omega_c^{i_c}} \left(1 - \sum_{j=1}^{n_p} b_j \varphi_j - \sum_{j=1}^{n_p} \Psi_{1,j} \varphi_j - \sum_{j=1}^{n_p} \Psi_{4,j} \varphi_j \right) (k_2 n_{i_c} + k_1 (1 - n_{i_c})) g_{i_c, x}^2 \varphi_i \, d\Omega_c \\ &= \sum_{j=1}^{n_p} \sum_{i_c=1}^{n_f} (1 - b_j - \Psi_{1,j} - \Psi_{4,j}) (k_2 n_{i_c} + k_1 (1 - n_{i_c})) g_{i_c, x}^2 \int_{\Omega_c^{i_c}} \varphi_i \varphi_j \, d\Omega_c. \end{aligned} \quad (3.41)$$

Since the cell may not be contained in a single element, the evaluation of the integral $\int_{\Omega_c^{i_c}} \varphi_i \varphi_j \, d\Omega_c$ may prove to be problematic. Therefore, we approximate this integral by using the cell center \underline{x}_{i_c} and its corresponding area:

$$\int_{\Omega_c^{i_c}} \varphi_i \varphi_j \, d\Omega_c \approx \mathcal{A}(\Omega_c^{i_c}) \varphi_i(\underline{x}_{i_c}) \varphi_j(\underline{x}_{i_c}). \quad (3.42)$$

The same is done for the equation concerning Ψ_{yy} .

3.3.3. CONTRACTION

Our main interest is the implementation of contraction. Therefore, we derive the Galerkin equations that are solved in order to find the displacement. We start with the temporary, contractile forces from a single (myo)fibroblast and choose the test function to be φ_i with $i \in \{1, \dots, n_p\}$. Equation (2.84) then becomes:

$$\int_{\Omega_t} \varphi_i \underline{F}_{temp} \, d\Omega_t = \int_{\Omega_t} -2r_s \rho_c P_0 \begin{bmatrix} \delta(\underline{x} - \underline{x}_c^E) - \delta(\underline{x} - \underline{x}_c^W) \\ \delta(\underline{x} - \underline{x}_c^N) - \delta(\underline{x} - \underline{x}_c^S) \end{bmatrix} \varphi_i \, d\Omega_t \quad (3.43)$$

$$= -2r_s P_0 \begin{bmatrix} \rho_c(\underline{x}_c^E) \varphi_i(\underline{x}_c^E) - \rho_c(\underline{x}_c^W) \varphi_i(\underline{x}_c^W) \\ \rho_c(\underline{x}_c^N) \varphi_i(\underline{x}_c^N) - \rho_c(\underline{x}_c^S) \varphi_i(\underline{x}_c^S) \end{bmatrix}. \quad (3.44)$$

By finding which element contains each of the midpoints, the corresponding values of the collagen density and the test functions at the cell positions can be determined. With these relations, equation (3.44) is evaluated.

The second type of contractile force we consider are plastic forces. As shown in Section 2.2.4, these are also formulated using Dirac delta functions. Therefore, choosing φ_i the same as in the previous derivation, we obtain the following for the plastic forces on element e :

$$\begin{aligned} \int_{\Omega_t} \varphi_i \underline{F}_{pt}^e \, d\Omega_t &= \int_{\Omega_t} \varphi_i \sum_{j=1}^3 P(\tau_e) \underline{n}(\underline{x}_j^e) \delta(\underline{x} - \underline{x}_j^e) \Delta l_j \, d\Omega_t \\ &= \sum_{j=1}^3 P(\tau_e) \underline{n}(\underline{x}_j^e) \varphi_i(\underline{x}_j^e) \Delta l_j. \end{aligned} \quad (3.45)$$

We now define \underline{x}_j^e to be the midpoint opposite of the node e_j . Since we use piecewise linear func-

tions, we obtain:

$$\phi_i(\underline{x}_j^e) = \frac{1}{2}(1 - \delta_{i,e_j}), \quad (3.46)$$

in which $\delta_{i,j}$ is the Kronecker delta function. Substituting this into equation (3.45), we arrive at:

$$\int_{\Omega_t} \varphi_i \underline{F}_{pl}^e d\Omega_t = \sum_{j=1}^3 P(\tau_e) \underline{n}(\underline{x}_j^e) \frac{1}{2}(1 - \delta_{i,e_j}) \Delta l_j \quad (3.47)$$

Applying the superposition principle, in which we assume n_f fibroblasts and myofibroblasts and n_e triangular elements, the terms concerning the forces in the Galerkin equations for the mechanical balance in equation (2.51) read as follows:

$$\int_{\Omega_t} \varphi_i \underline{g} d\Omega_t = \sum_{k=1}^{n_f} \left(-2r_s P_0^k \begin{bmatrix} \rho_c(\underline{x}_k^E) \varphi_i(\underline{x}_k^E) - \rho_c(\underline{x}_k^W) \varphi_i(\underline{x}_k^W) \\ \rho_c(\underline{x}_k^N) \varphi_i(\underline{x}_k^N) - \rho_c(\underline{x}_k^S) \varphi_i(\underline{x}_k^S) \end{bmatrix} \right) + \sum_{e=1}^{n_e} \left(\sum_{j=1}^3 P(\tau_e) \underline{n}(\underline{x}_j^e) \frac{1}{2}(1 - \delta_{i,e_j}) \Delta l_j \right). \quad (3.48)$$

To finalize the formulation, we approximate u and v using linear elements by substituting $u = \sum_{j=1}^{n_p} u_j \phi_j$ and $v = \sum_{j=1}^{n_p} v_j \phi_j$ in equation (2.68):

$$\begin{aligned} \sum_j u_j \left[\int_{\Gamma \setminus \Gamma^N} s \rho_c \varphi_j \varphi_i d\Gamma + \frac{E}{(1+\nu)(1-2\nu)} \int_{\Omega_t} (1-\nu) \frac{\partial \varphi_j}{\partial x} \frac{\partial \varphi_i}{\partial x} + (1-2\nu) \frac{1}{2} \frac{\partial \varphi_j}{\partial y} \frac{\partial \varphi_i}{\partial y} d\Omega_t \right] + \\ \sum_j v_j \left[\frac{E}{(1+\nu)(1-2\nu)} \int_{\Omega_t} \nu \frac{\partial \varphi_j}{\partial y} \frac{\partial \varphi_i}{\partial x} + \frac{1}{2}(1-2\nu) \frac{\partial \varphi_j}{\partial x} \frac{\partial \varphi_i}{\partial y} d\Omega_t \right] = \int_{\Omega_t} g_1 \varphi_i d\Omega_t. \end{aligned} \quad (3.49)$$

The same derivation is done for equation (2.69) for which we obtain the following:

$$\begin{aligned} \sum_j v_j \left(\int_{\Gamma \setminus \Gamma^N} s \rho_c \varphi_j \varphi_i d\Gamma + \frac{E}{(1+\nu)(1-2\nu)} \int_{\Omega_t} (1-2\nu) \frac{1}{2} \frac{\partial \varphi_j}{\partial x} \frac{\partial \varphi_i}{\partial x} + (1-\nu) \frac{\partial \varphi_j}{\partial y} \frac{\partial \varphi_i}{\partial y} d\Omega_t \right) + \\ \sum_j u_j \frac{E}{(1+\nu)(1-2\nu)} \left(\int_{\Omega_t} (1-2\nu) \frac{1}{2} \frac{\partial \varphi_j}{\partial y} \frac{\partial \varphi_i}{\partial x} + \nu \frac{\partial \varphi_j}{\partial x} \frac{\partial \varphi_i}{\partial y} d\Omega_t \right) = \int_{\Omega_t} g_2 \varphi_i d\Omega_t. \end{aligned} \quad (3.50)$$

This concludes the formulation of the Galerkin equations which we solve to obtain the displacements.

3.4. INTERACTION BETWEEN CONTINUUM AND DISCRETE ENTITIES

Processes such as cell movement and receptor binding strongly depend on the values of fiber densities and cytokine concentrations. Since these entities are only defined on the mesh points in the domain and not necessarily at the position of a cell, an interpolation scheme needs to be introduced.

Let us consider interpolating a general quantity η to obtain the value at the position of a cell \underline{x}_c .

By using linear interpolation, we approximate the values for the continuum quantities using linear basis functions:

$$\eta(\underline{x}) = \sum_{j=1}^{n_p} \eta_j \varphi_j(\underline{x}). \quad (3.51)$$

To use this efficiently, we find the element e which contains the center of the cell. Let us denote the nodes of e by e_1 , e_2 and e_3 . On this element, the only nonzero basis functions φ_{e_1} , φ_{e_2} , and φ_{e_3} . We can now use equation (3.51) and simplify it to the following:

$$\eta(\underline{x}_c) = \sum_{j=1}^3 \eta_{e_j} \varphi_{e_j}(\underline{x}_c) = \begin{bmatrix} \varphi_{e_1}(\underline{x}_c) & \varphi_{e_2}(\underline{x}_c) & \varphi_{e_3}(\underline{x}_c) \end{bmatrix} \begin{bmatrix} \eta_{e_1} \\ \eta_{e_2} \\ \eta_{e_3} \end{bmatrix}. \quad (3.52)$$

With this, we can create an interpolation matrix X_c in order to interpolate the values to all cell positions. Now, the interpolation scheme has been simplified to a matrix-vector multiplication:

$$\underline{\eta}_c = X_c \underline{\eta}. \quad (3.53)$$

3.5. TIME INTEGRATION SCHEME

In order to calculate the values corresponding to all species at the next time step, we use a time integration scheme. Due to the complexity of a moving mesh, the discrete entities are calculated using an explicit forward Euler scheme. When these values are known, the remaining calculations are done using a backward Euler scheme in order to ensure stability. The entire scheme can be summarized to the following:

1. Explicit section
 - (a) Calculate displacement due to contractile forces from (myo)fibroblasts. These forces are based on the current values of collagen density and the values of the artificial time τ .
 - (b) Calculate cell velocities using the current values of bound receptors, interpolated values of PDGF and TGF- β concentrations, and fibrin and collagen densities. For both types of fibroblasts, contact guidance by collagen bundles is incorporated as well. The interpolation is done as explained in Section 3.4.
 - (c) Create new cell positions \underline{x}_c^{i+1} by using cell velocities, convective fluxes from the moving tissue and the contact forces created by collisions.
 - (d) Mitosis occurs once the criteria are met and new fibroblasts are introduced. These criteria are based on current values of bound receptors and the experienced cell density. A cell introduced by mitosis inherits the status of myofibroblast from its parent. Fibroblast decay is incorporated as well using samples from exponential distributions as explained in Section 2.1.9.
 - (e) Introduce leukocytes on the wound boundary as the PDGF concentration increases.

Leukocyte decay is calculated as well which strongly depends on the concentration of PDGF as shown in section 2.1.9.

- (f) Update mesh points \underline{x}_p^{i+1} according to displacement. With this updated mesh, the new test function φ is formulated which will be used in the implicit section.

2. Implicit section

- (a) PDGF concentration is calculated using a simple diffusion equation and the added deformation terms.
- (b) tPA and fibrin concentrations are calculated using Picard iteration as explained in Algorithm 3.2.
- (c) Create the source function for TGF- β based on the new coordinates of leukocytes and corresponding fibrin densities. With this function and the incorporated deformation, the concentration of TGF- β is updated.
- (d) Update receptor values of leukocytes and fibroblasts based on interpolated values of PDGF and TGF- β .
- (e) The synthesis of collagen bundles is determined based on new fibroblast positions, the corresponding receptor values, and the interpolated values of collagen and fibrin density.

4

RESULTS AND DISCUSSION

In this chapter, the obtained results are discussed. We focus on various aspects of the model and demonstrate what the influences are of the stochastic components and contractile forces on the wound healing process. First, the process of fibrin decay is considered and we present how the fibrin-rich clot is broken down. Second, we look at the production of cytokines and show how the concentrations of these cytokines change during the different stages of the wound healing process. Third, the cell populations inside the wound space are considered. Fourth, the process of the synthesis of collagen within the wound site is considered. Here we focus on both the density and the degree of isotropy of the newly formed collagen bundles. Fifth, the results from the addition of contraction are presented. Sixth, an overview is given of the entire process. Here we focus on cell movement, collagen synthesis and contraction. Finally, we show what the influence is of an increase in temporal forces and plastic forces on the outcome of the healing process. A list of parameter values used in the simulations can be found in Appendix A.

4.1. FIBRIN DYNAMICS

As explained in Section 2.1.2, the only two species associated with this process are tPA fibrin. In order to show the decrease in the total amount of fibrin, we look at the average fibrin density over the domain. This value can be obtained using the following formula:

$$\bar{\rho}_f^n = \frac{\int_{\Omega_t^n} \rho_f(\underline{x}, t_n) d\Omega_t^n}{\mathcal{A}(\Omega_t^n)}, \quad (4.1)$$

in which Ω_t^n is the dynamic domain at time t_n .

The results are shown in Figure 4.1. According to Enoch and Leaper (2008), the fibrin clot is removed during the proliferative phase which lasts from day 3 until approximately 2-4 weeks after wounding. In the results obtained from the model, we see that the fibrin decay starts relatively early in the initial stages of the wound healing process. This is due to the constant tPA production assumed in the model. It is more important, however, at what time the fibrin clot has completely decayed since this marks the end of its influence on both cell movement and TGF- β production. It is shown that the entire clot is removed within the first 10 days after wounding. This matches correctly with the expected breakdown in the proliferative phase.

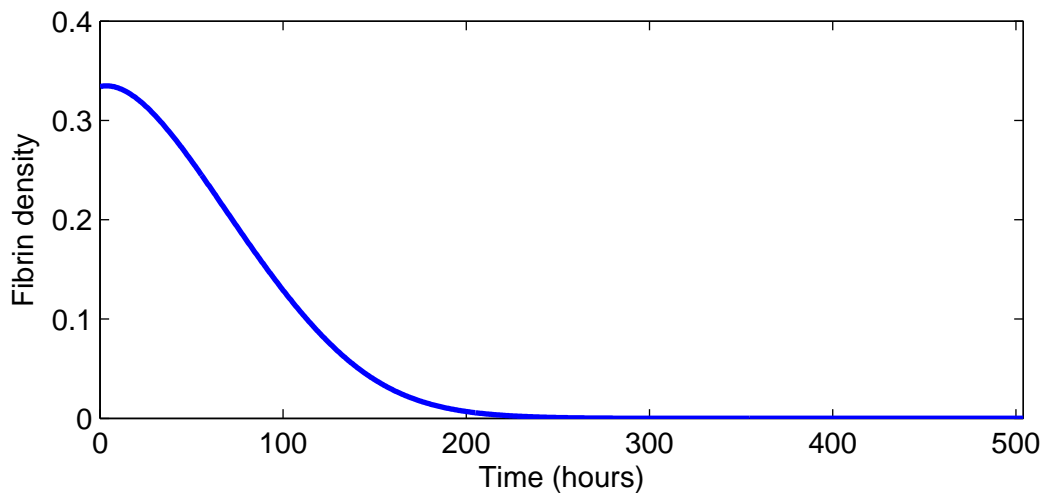


Figure 4.1: The average fibrin density within the domain of computation throughout time. Note that the fibrin-rich clot which initially occupies the wound space, is removed during the first 10 days of the wound healing process.

With respect to spatial dynamics, we show the results in Figure 4.2. Here, we note that the tPA production at the edges of the wound result in a breakdown of the clot which starts at the wound edges and proceeds towards the center of the wound. The breakdown is shown in the first 200 hours. Note that the first signs of contraction can be seen at the top of the domain as well which will be elaborated upon in Section 4.5.

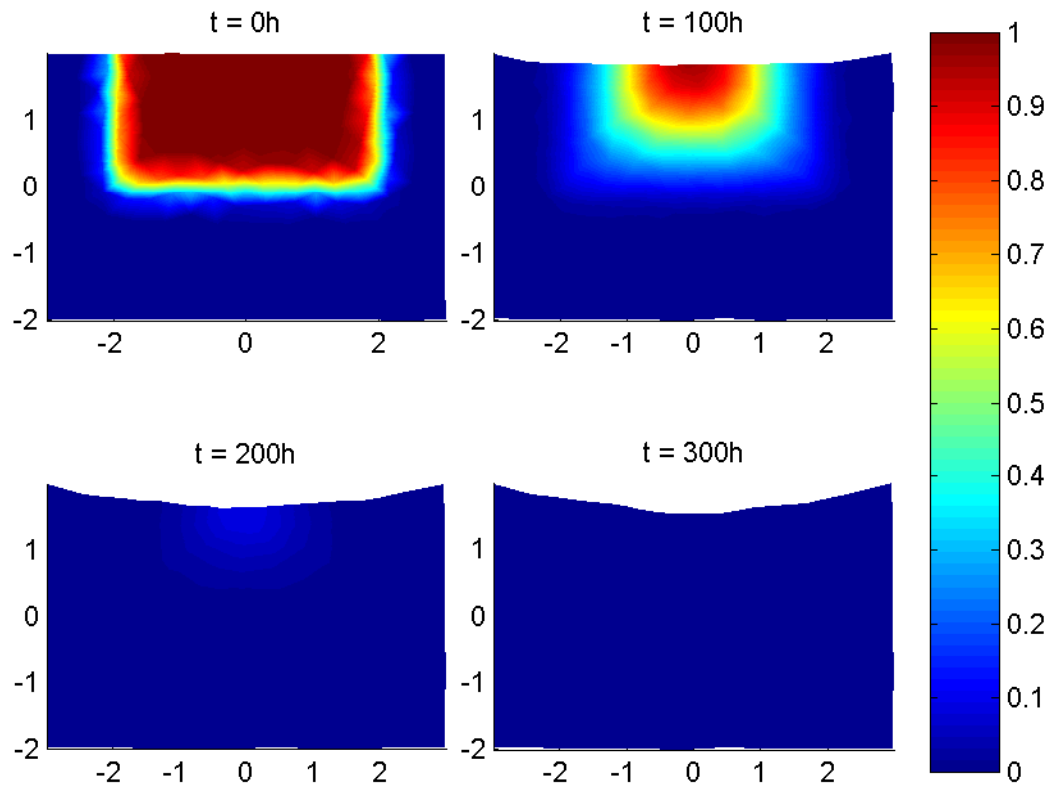


Figure 4.2: The dynamics of the fibrin density at consecutive times in a single model run. We see that the clot is broken down from the wound edges towards the center of the wound.

4.2. CYTOKINE PRODUCTION

The second result we discuss concerns the changes in cytokine concentrations throughout time. Let us first consider the concentration of PDGF which simply diffuses from the wound space into the surrounding tissue. The average PDGF concentration is calculated in a similar manner to the average fibrin density and is shown in Figure 4.3. We note that the peak in PDGF concentration is

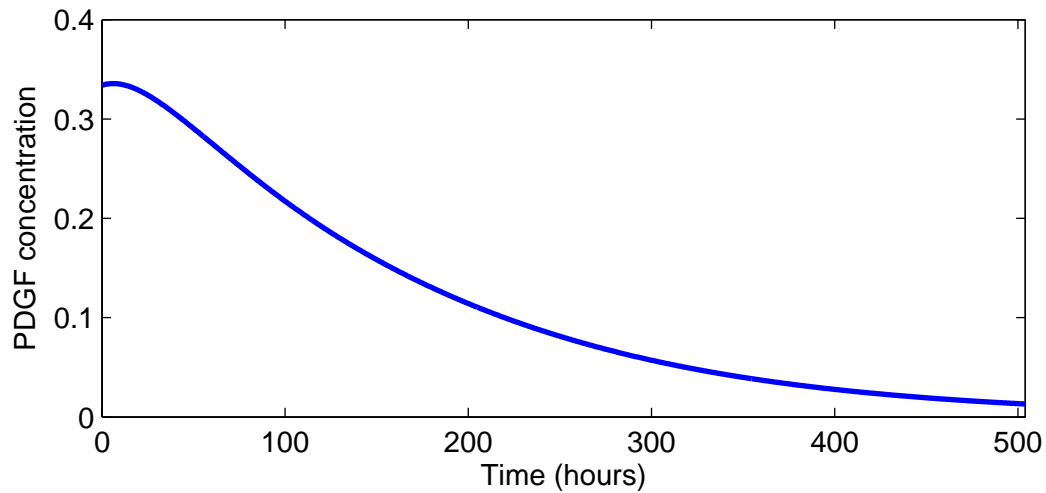


Figure 4.3: The average PDGF concentration within the domain of computation throughout time. Note that this cytokine slowly diffuses into the surrounding, undamaged tissue in order to attract leukocytes.

early in the inflammatory phase. This is to be expected from a modeling point of view since there is no production of this cytokine in the model. PDGF fulfills the role of chemoattractant for leukocytes in this model and since leukocytes should arrive in the inflammatory phase, this early peak in PDGF concentration is a desired result.

Figure 4.4 shows how the spatial profile of PDGF changes throughout time. Note that the cytokine is mostly present in the wound site initially and diffuses quickly to the surrounding tissue. A direct effect of this diffusion is the arrival of leukocytes which will be discussed in Section 4.3.

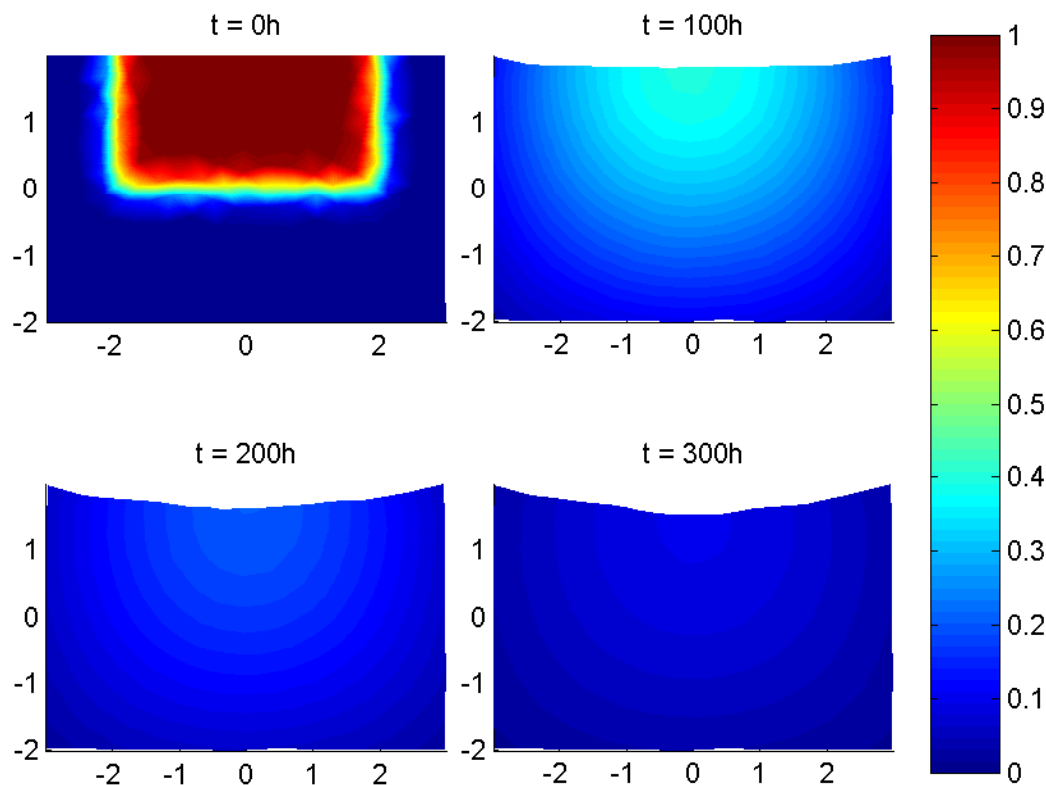


Figure 4.4: The dynamics in PDGF concentration throughout time. The cytokine quickly diffuses from the wound site into the surrounding tissue in order to attract leukocytes.

The second cytokine profile we consider is the concentration of TGF- β which is calculated similar to equation (4.1). This cytokine is produced by leukocytes and due to the stochastic terms associated with leukocyte arrival and decay, its profile changes between different model runs. Therefore, Figure 4.5 shows the 5th percentile, mean and 95th percentile of 100 model simulations over time.

Even though there is a certain deviation from the mean, we see that the peak in TGF- β concentration is always approximately five days after wounding. Since this cytokine acts as a chemoattractant for both myofibroblasts and fibroblasts, this peak is to be expected early in the proliferative phase. The proliferative phase starts approximately on day three (Enoch and Leaper, 2008) which means that this result is in line with our expectations.

To give an insight into the spatial profile of TGF- β throughout time, Figure 4.6 shows the results from a single model run. Here we see that the production by leukocytes creates a peak in TGF- β concentration inside the wound space. Afterwards, as the production decreases, this peak decreases as well due to diffusion.

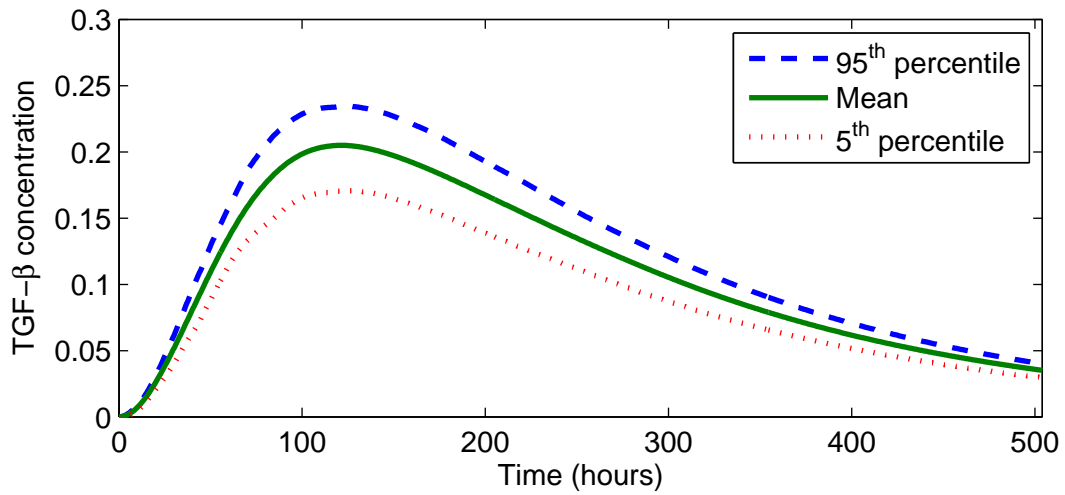


Figure 4.5: The 5th percentile, mean and 95th percentile at each time step of 100 simulations. We see that the deviation from the mean only concerns the height of the peak and not the moment in time at which it occurs.

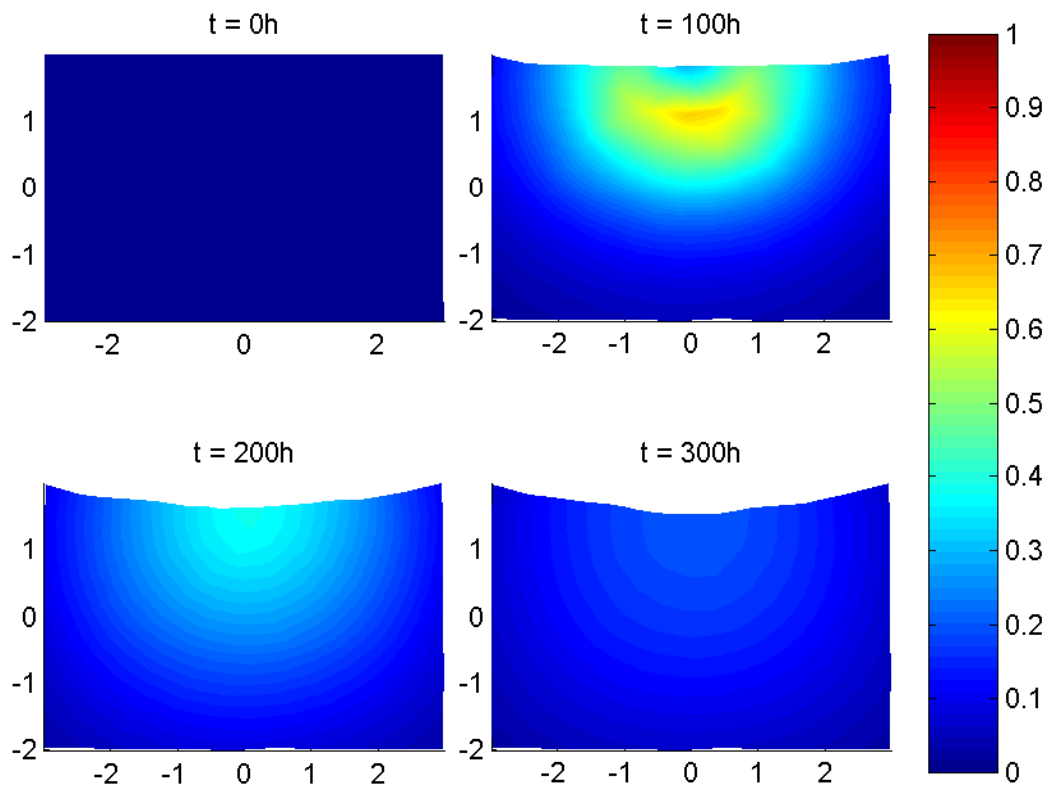


Figure 4.6: The TGF- β profile throughout time shows that the peak, which occurs at approximately day 5, lies within the wound space.

4.3. CELL POPULATIONS

As explained in Section 1.1, the several stages of wound healing are marked by the presence of different types of cells in the wound space. In order to present these stages within this model, we turn to the number of cells in the wound area at each time step. Since both myofibroblasts and fibroblasts arrive at the same time in this model, we do not distinguish between them in these results.

Figure 4.7 shows the size of the different cell populations throughout time in which two distinct peaks can be seen. First, after approximately two days, the number of leukocytes spikes since these are the first to be attracted towards the damaged tissue. Their arrival marks the inflammatory phase in which they start producing TGF- β . Again, this corresponds to the inflammatory phase as described by (Enoch and Leaper, 2008).

Second, the steady arrival of fibroblasts occurs. After approximately five days, the fibroblasts form the majority of the two cell species in the wound area which can be seen as the transition from the inflammatory phase to the proliferative phase. The fibroblast population reaches its peak at approximately 12 days after wounding. This matches well with the time period which Enoch and Leaper (2008) presents, which states that the peak occurs between the tenth and the twenty-first days.

Afterwards, these cells decay as well which is typical for the remodeling and maturation phase (Enoch and Leaper, 2008).

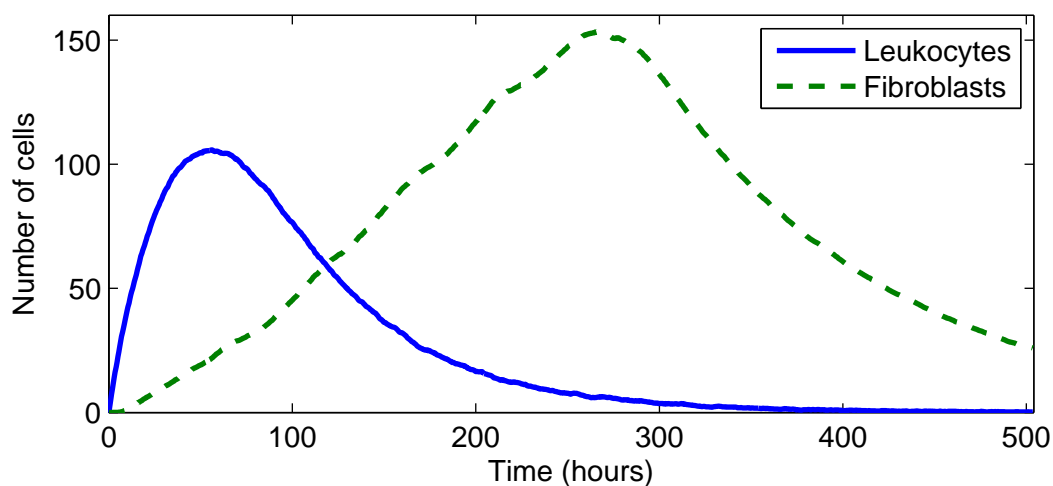


Figure 4.7: The number of leukocytes and fibroblasts in the wound space throughout time. The distinction between two phases in the process is made by noting which cell species forms the majority.

Due to the stochastic terms within this model, a certain deviation is to be expected between different model runs. In order to show the size of this deviation, the population results after several runs are displayed in Figure 4.8.

From this figure, we conclude that the deviation in the number of leukocytes is relatively small. Naturally, this is a desired effect since it implies that the stochastic terms concerning the introduction

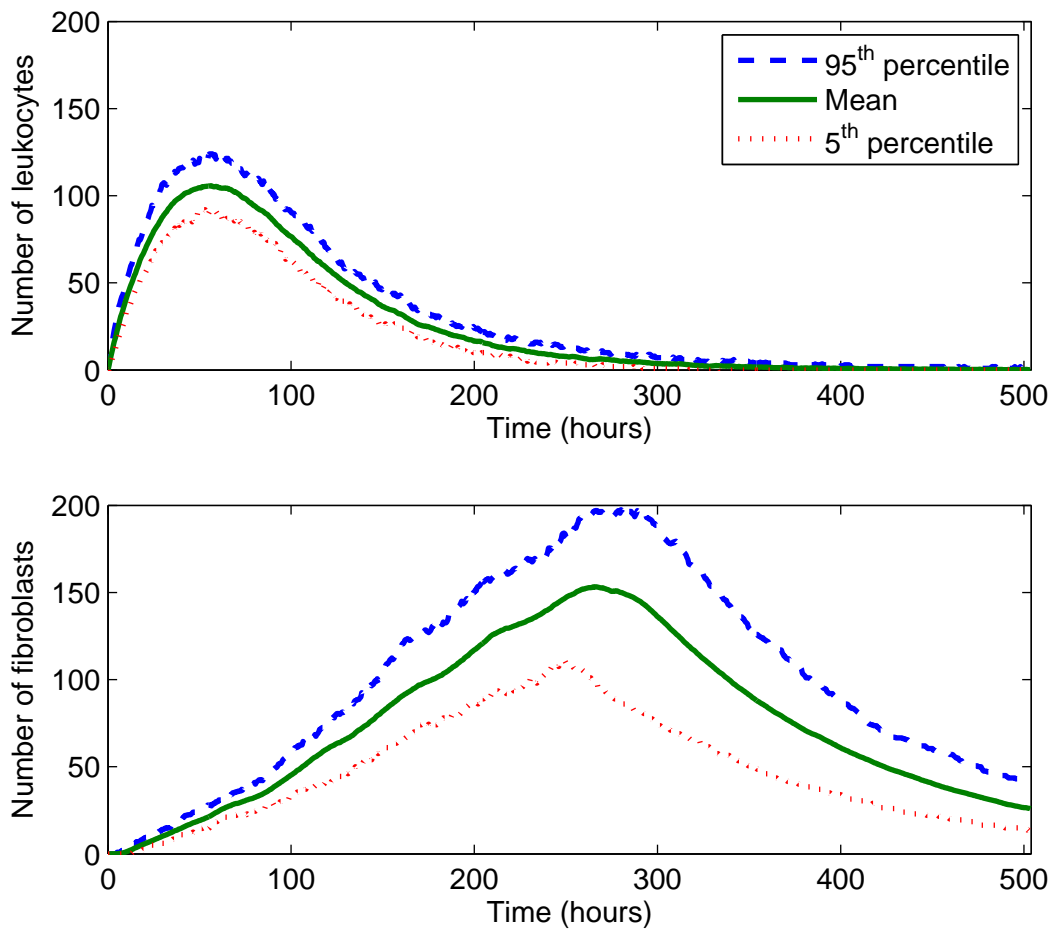


Figure 4.8: The 5th percentile, mean and 95th percentile of the number of leukocytes and fibroblasts in the wound space at each time step. The deviation concerning the fibroblast population is significantly larger than the deviation in leukocyte population. Nevertheless, the two peaks marking the different stages of wound healing can be seen clearly.

and decay of leukocytes are well-tuned and do not introduce any significant deviations.

On the other hand, the peak in fibroblast population deviates more, both in time as in the number of cells. This is due to the fact that the decay of fibroblasts is modeled using stochastic terms while the initial number of fibroblasts and the process of mitosis are modeled deterministically. A large number of cell deaths in the initial stages of the simulation can therefore cause relatively large deviations of the peak. The effect this deviation has on the remainder of the model will be determined in the following sections.

4.4. COLLAGEN SYNTHESIS

The first influence a deviation in cell populations has is on the production of collagen. This process depends on the number of (myo)fibroblasts since these are the types of cells which produce and reorient collagen bundles. In Figure 4.9, we present the results of the average collagen density in the entire wound space.

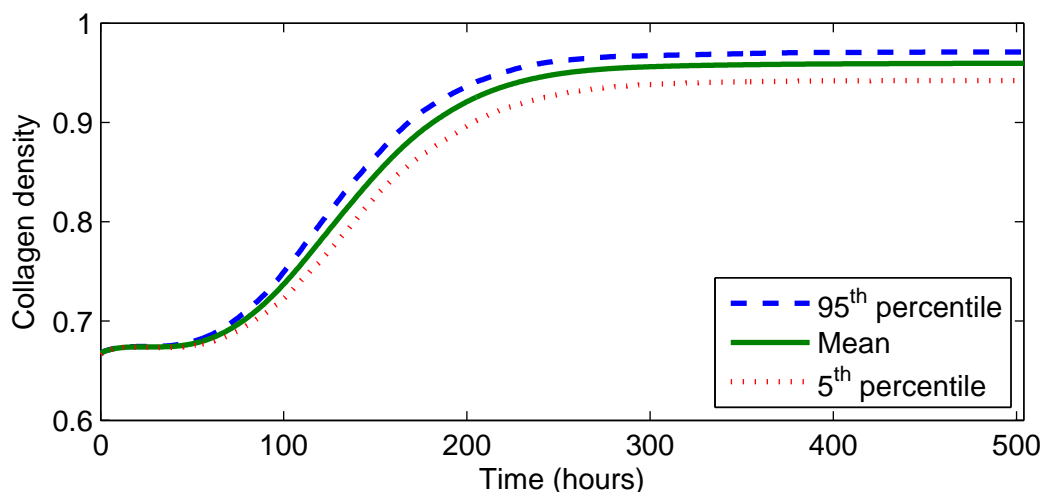


Figure 4.9: The 5th percentile, mean and 95th percentile of the average collagen density in the domain during each time step. The highest increase in collagen density occurs once the fibrin clot is broken down and the first fibroblasts arrive.

These results show that collagen production starts after three days, which once again corresponds to the theory explained by Enoch and Leaper (2008). The density then increases to its maximum value during the proliferative phase. Even though a high dependency on the population of (myo)fibroblasts might be expected, the deviation here is relatively small. The reason for this is that the number of (myo)fibroblasts is sufficient in all model runs. The synthesis of collagen fibers is halted once the density reaches its maximum. Therefore, the (myo)fibroblasts that arrive after most of the collagen bundles have been synthesized, will have little influence on the collagen density.

To illustrate the production of collagen, Figure 4.10 shows the collagen density at consecutive times. Initially, the density increases along the wound edges since this is where the fibroblasts and myofibroblasts enter the wound site. As they migrate towards the center of the wound, their receptors bind to the cytokine TGF- β which results in an increase in collagen production.

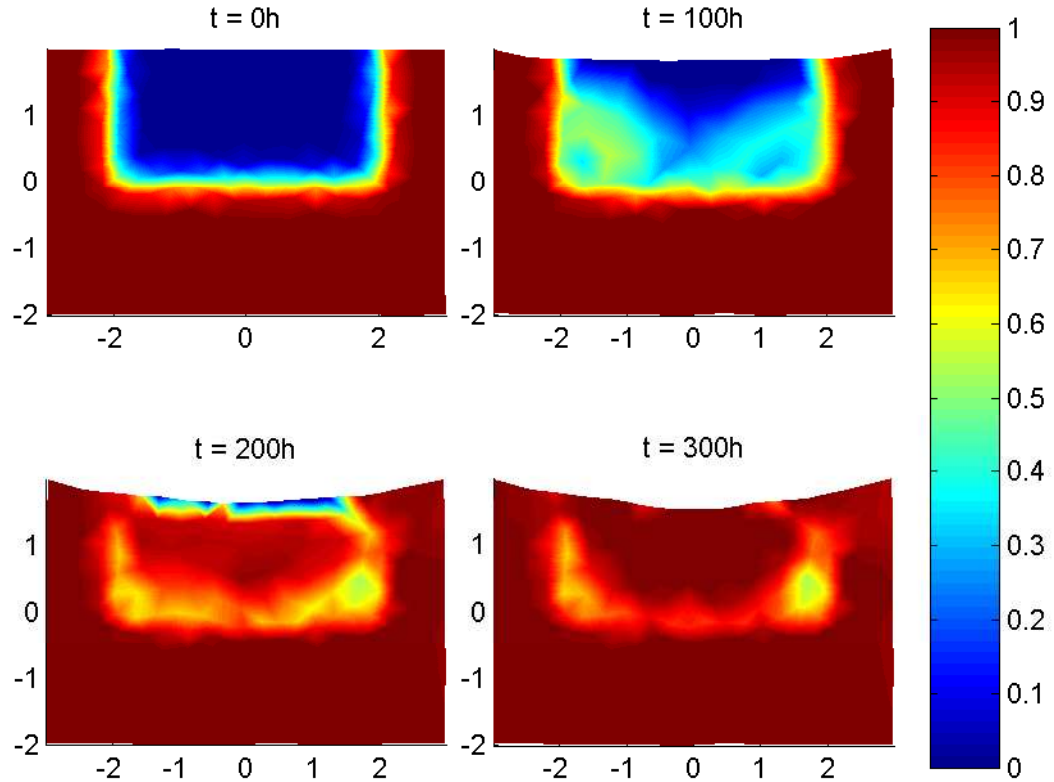


Figure 4.10: The collagen density in the domain throughout time. The wound site is filled with collagen fibers synthesized by fibroblasts and myofibroblasts which arrive from the surrounding tissue. After 300 hours, some lighter areas can be seen which mark a lower collagen density. This is mostly due to the lower collagen synthesis by arriving (myo)fibroblasts.

Besides being interested in the collagen density, the isotropy of collagen fibers provides another property of the wound area. To investigate this property, we use the tensorial approach to collagen fibers to our advantage. In this approach, the ratio between the eigenvalues can be used to form a measure of anisotropy in the wound. As proposed in Cumming et al. (2010), we will use the following measure e :

$$e = 1 - \frac{\lambda_2}{\lambda_1}, \quad (4.2)$$

in which λ_1 and λ_2 are the largest and smallest eigenvalues of the tensor Ψ , respectively. A small value of e implies a high degree of isotropy while a value close to one indicates a high degree of anisotropy. Figure 4.11 shows the anisotropy of collagen bundles in the domain throughout time. It is clear that the wound space is filled up with aligned fibers while the surrounding, uninjured tissue remains isotropic.

Analogous to the cytokine concentrations, we also present the average anisotropy of the collagen fibers in the domain throughout time. Once again, this is calculated analogous to equation (4.1). The result is shown in Figure 4.12. Note that the degree of anisotropy is established relatively early

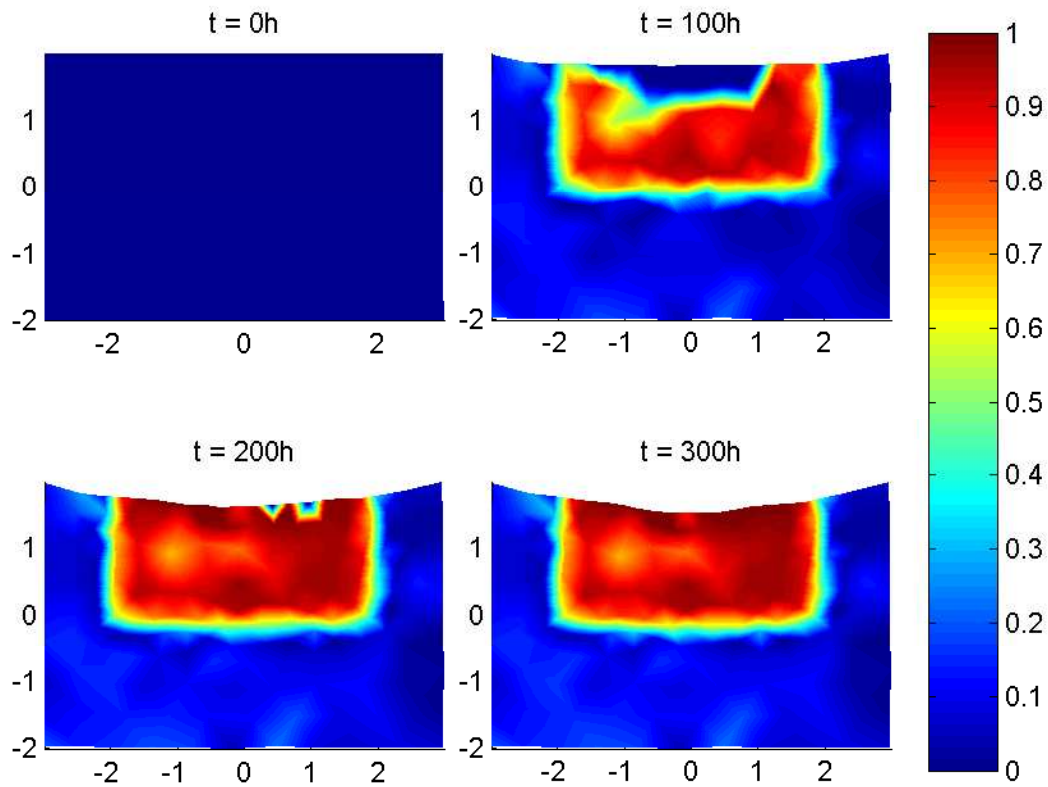


Figure 4.11: The anisotropy of collagen bundles in the domain throughout time. A large difference can be seen between the isotropic tissue in blue which surrounds the wound area and the newly formed collagen fibers in the wound area which are shown in red due to anisotropy.

compared to the collagen density. The reason for this is that most fibroblasts and myofibroblasts travel the same paths due to the gradient of the chemoattractant and contact guidance. As a consequence, the collagen fibers which are synthesized by these (myo)fibroblasts will lie in the same direction. The addition of these fibers only changes the density and not the degree of anisotropy.

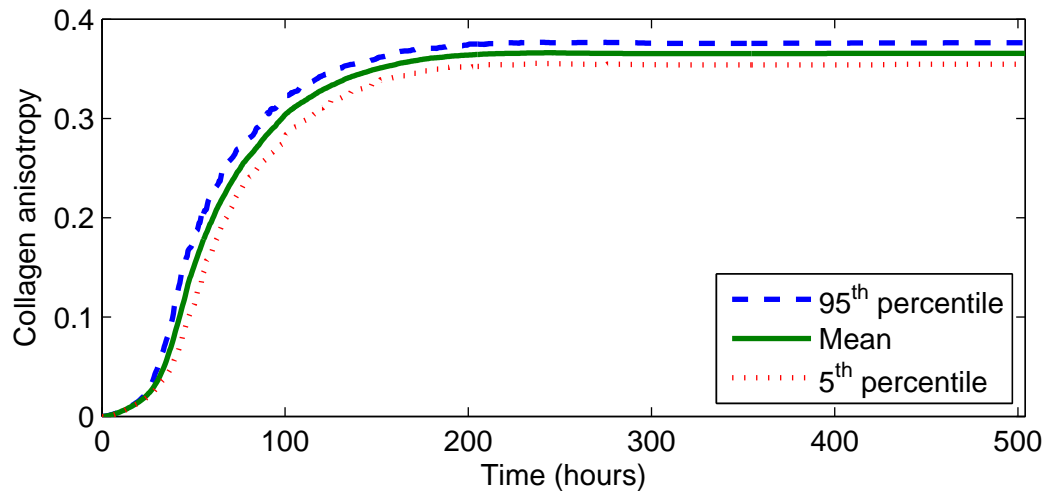


Figure 4.12: The anisotropy of collagen bundles in the domain throughout time.

4.5. CONTRACTION

In order to calculate the amount of contraction in the wound, a measure of contraction is needed. Let us denote the wound space at time $t = t_n$ with Ω_w^n . The area of the wound space at this time will then be denoted by $\mathcal{A}(\Omega_w^n)$. The required measure must be relative to the initial area of the wound space to enable comparison to other wounds. By dividing the current area of the wound space by its initial area, we obtain this measure A^n :

$$A^n = \frac{\mathcal{A}(\Omega_w^n)}{\mathcal{A}(\Omega_w^0)}. \quad (4.3)$$

We present the results concerning the area of the wound with the use of this measure in Figure 4.13. Note that the area is first increased which is due to the contractile forces of cells in the surrounding tissue. Then, after approximately four days, the arrival of (myo)fibroblasts which we have seen in Section 4.3 causes contraction inside the wound space. In accordance with Clark (2014), a significant decrease starts approximately at the beginning of the second week.

After approximately two weeks, fibroblast decay causes a decrease in temporary forces and only plastic forces remain. Due to these plastic forces, the contracture in the wound remains which is represented by the horizontal tail in Figure 4.13.

When we compare different model runs, we notice a certain deviation in this process of contraction as well. This is a direct effect from the deviation in the number of arriving myofibroblasts and fibroblasts, since these are the cells responsible for all contractile forces. However, the difference in the degree of contracture is only influenced by the amount of myofibroblasts which enter the wound area.

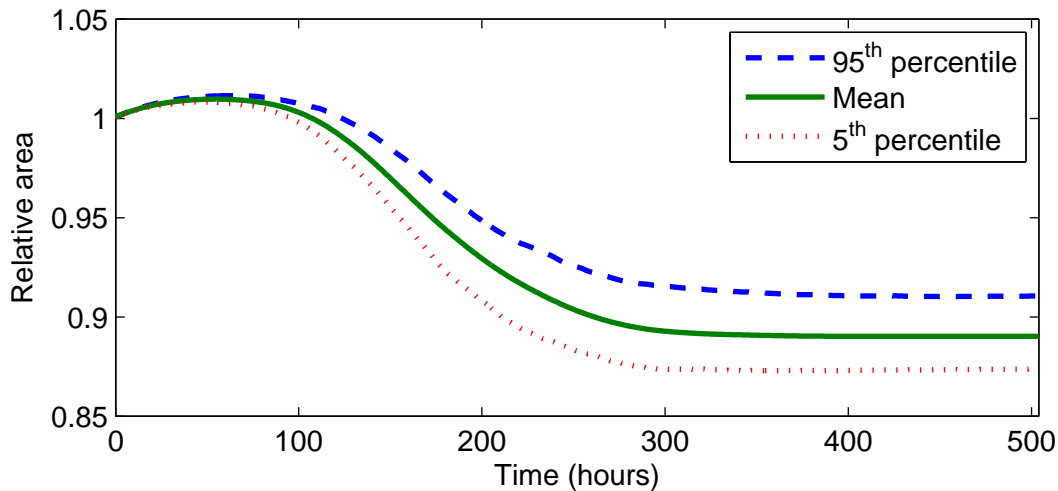


Figure 4.13: The 5th percentile, mean and 95th percentile of the area of the wound space during each time step. A small, initial increase can be seen due to contractile forces outside the wound space. This is followed by a large decrease in area as fibroblasts enter the wound space, produce collagen and exert both temporary and plastic forces here. Finally, the contracture can be seen by the constant area in the final stages of the simulation.

4.6. CELL MOVEMENT

In order to present the results concerning cell movement, Figure 4.14 gives a view at consecutive times during the wound healing process. In this figure, we clearly see the initial population of fibroblasts and myofibroblasts in the surrounding tissue. Collagen is represented by black crosses which point in the direction of the eigenvalues of the corresponding tensor. The lengths of the axes of the cross represent the collagen density while the ratio between the axes represents the dominance of one direction over the other.

After four days, the wound space is occupied by both leukocytes and (myo)fibroblasts. Note how the number of leukocytes has increased significantly within these first four days. Furthermore, the wound area has been stretched out slightly by the contractile forces exerted in the surrounding tissue as we have seen in Section 4.5. At the top of the domain, the first signs of contraction at the skin surface can be seen.

In the third frame, the state of the domain after eight days is shown. At this moment, we see that the first collagen bundles have been synthesized in the wound area. A vast majority of the (myo)fibroblasts has entered the wound space while we observe a significant decrease in the amount of leukocytes.

After twelve days, we see that the (myo)fibroblasts have started to group together and proliferated through the process of mitosis. Due to the large amount of contractile forces which accompany such a large population, the skin surface has deformed significantly compared to earlier stages.

In the final eight days, the model shows a steady decrease in (myo)fibroblast population which reveals an oriented collagen pattern underneath. The newly synthesized fibers inside the wound

space are oriented towards the center of the wound.

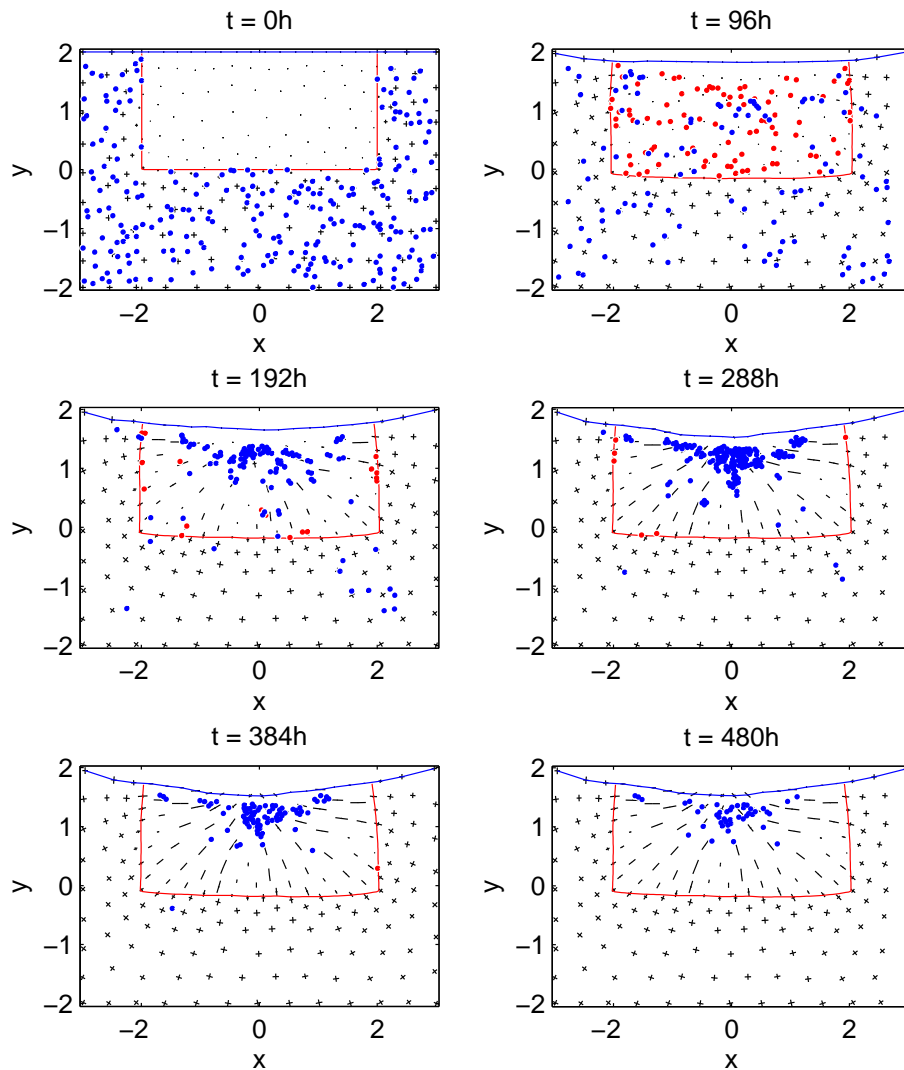


Figure 4.14: Cell positions, orientation of collagen fibers and the borders of the domain and wound space consecutive times. Fibroblasts and myofibroblasts and leukocytes are represented in blue and red, respectively. Collagen fibers are shown in black in which the crosses are aligned with the eigenvectors of the tensor.

Figure 4.15 shows the final state of the domain three weeks after wounding. We see a contracted state in which the top boundary has deformed into a curved shape. This deformation remains after all cells have died or left the area which is typical for a contracture. Furthermore, there is a large difference in the degree of isotropy between the wound space and the surrounding tissue. In the wound space, all bundles are oriented towards the center of the wound. In the surrounding tissue, an isotropic pattern remains which is represented by crosses with equal arms.

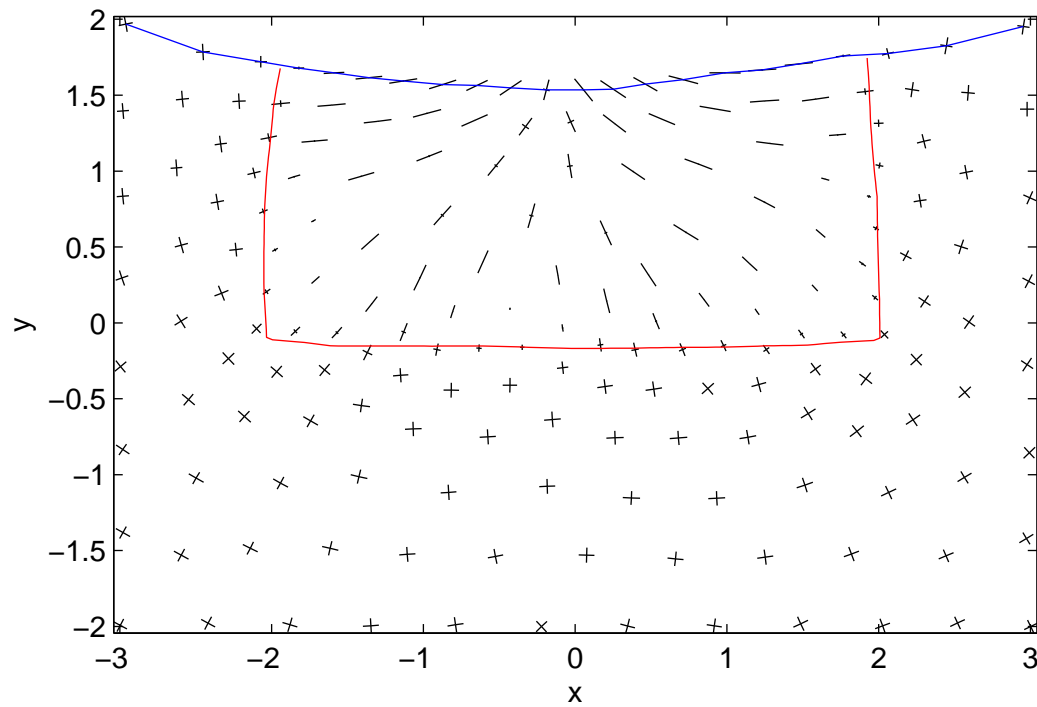


Figure 4.15: A typical final state of the domain after three weeks. Note that the contracture is shown here since it remains after all other processes are completed. Furthermore, the difference in isotropy in collagen bundles can be seen between the wound space and the surrounding tissue.

4.7. INCREASE IN TEMPORARY FORCES

In order to show the difference between temporary forces and plastic forces, we consider a large increase in temporary forces by making them six times as large. Even though this increased force is not realistic, it will give an insight into the effect this force has, which is shown in Figure 4.16.

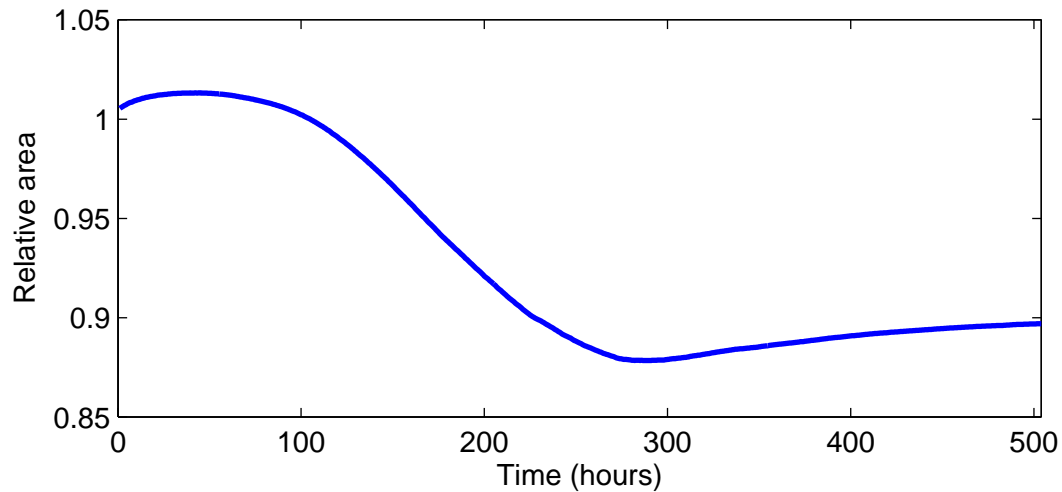


Figure 4.16: If the temporary forces are increased, the initial decrease of the wound area is greater. However, once the (myo)fibroblasts start to decay, the area increases to a steady state.

The alteration in temporary forces causes the area of the wound to contract to a smaller area within the first twelve days. This contraction is reversed however, once the fibroblasts and myofibroblasts start to decay. As shown in Section 4.3, these populations are almost completely removed after approximately 21 days. Because of this we see that the area of the wound increases slightly to a steady state. This steady state, which corresponds to a lower area than initially, represents the contracture in the wound.

Note that the degree of contracture is similar to the results discussed in Section 4.5. This implies that the temporary forces only influence the manner in which this contracture is established and not its degree.

4.8. INCREASE IN PLASTIC FORCES

By making the plastic forces more dominant, a dramatic increase in contracture can be seen. As shown in figure 4.17, the area is decreased to approximately 80% if the size of the plastic forces is doubled. Compared to the 90% we saw earlier, this shows that the size of the plastic forces directly influences the degree of contracture.

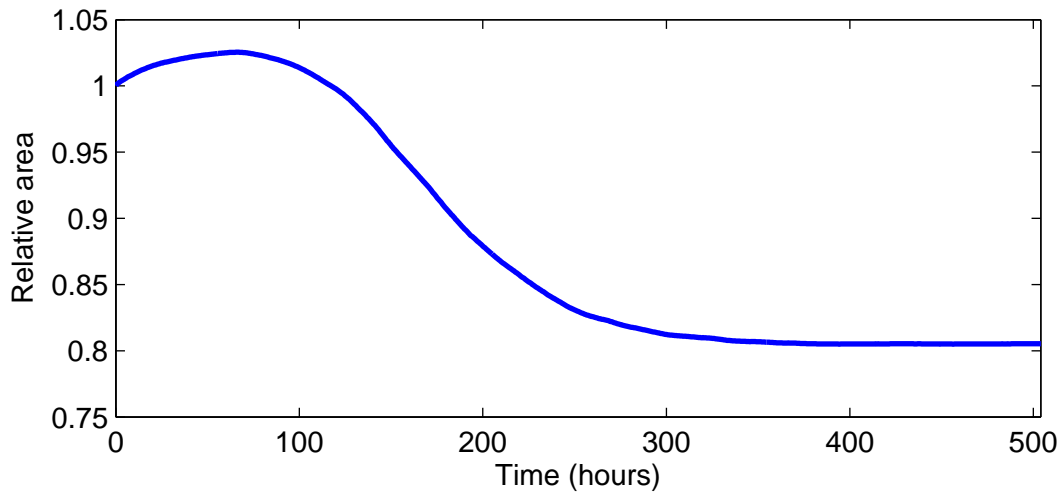


Figure 4.17: If the plastic forces are increased, the degree of contraction is increased as well. In this case, the plastic forces seem to completely dominate the temporary forces.

5

CONCLUSIONS

The objective of this project was to incorporate contraction and the formation of contracture in a biological model for dermal wound healing. In order to do this, we reevaluated the biological model presented by Cumming et al. (2010) and made several adjustments wherever necessary to incorporate this extension. For example, cells are represented as discrete discs moving through the dermis, which are in a continuous relationship with the continuum entities. This required the implementation of mobile source functions as well as interpolation between mesh points.

The mathematical formulation of the process of contraction was then presented, in which a distinction was made between temporary forces and permanent, plastic forces. In case of the temporary forces, the cells could not be considered as point forces and a novel formulation for contraction in all directions was presented. On the other hand, plastic forces were formulated in such a way that they remained even after the cell has left the area or died.

The continuous process of contraction results in a deformation during each time step. This deformation had a direct influence on all of the mediators in the model since the moving tissue introduced convective fluxes. The use of a moving mesh enabled us to calculate the dynamics of both continuum and discrete mediators.

The results obtained after incorporation of these mechanical components were shown in Chapter 4. We noted that the phases of wound healing were correctly represented and the order in which the various sub-processes took place matched well with the theory explained by Enoch and Leaper (2008). In short, we determined that the biological phenomena associated with dermal repair can be modeled mathematically using the governing equations we have presented and produce qualitatively sound results.

Most importantly, the process of contraction showed satisfactory results. First of all, the moments at which the process of contraction was initiated and completed during the wound healing process matched well with the theory. This is a crucial result because the correct timing of contraction is

critical for the wound healing process. For example, if contraction occurs for too long, it can result in disfigurement or loss of function (Hinz, 2006).

Second, the distinction between temporary and plastic forces allowed us to model deformation in the final phase of wound healing. When all fibroblasts and myofibroblasts had decayed, the plastic forces remained and caused a permanent deformation. This deformation represents contracture, which is precisely the aim of the model. To our knowledge, this model is the first of its kind to incorporate this formation of contracture during dermal wound healing.

6

RECOMMENDATIONS

In this section, we evaluate the model critically. We focus on both the incorporation of various components and their implementation within this model. Several suggestions are then presented to expand or adjust the model in order to make it more realistic.

First, let us consider the scale on which the calculations are made. The microscopic scale used in this model has a great advantage in describing the direct influences between discrete cells and the surrounding tissue. On the other hand, it cannot efficiently predict the wound healing process on a macroscopic scale. This means that it is not yet applicable to predict permanent contracture in wounds with a large area. Since contracture is the cause for major problems in larger wounds such as burn wounds, expanding this model to a larger scale is interesting.

Second, the distinction between fibroblasts and myofibroblasts was assumed to be static in this model. However, a myofibroblast is an activated type of fibroblasts which is achieved through differentiation. This differentiation was neglected in this model since we assumed both types of fibroblasts to be present in the surrounding tissue. A more realistic approach can be made by taking the differentiation from a fibroblast to a myofibroblast into account as well. As shown by Murphy et al. (2012) for example, this differentiation process could be triggered with the use of a cytokine such as TGF- β . In this model, we have considered TGF- β to be the activator for mitosis, not for differentiation.

Third, we have assumed that myofibroblasts are constantly active. However, this assumption contradicts the current understanding of the activation of myofibroblasts. According to Wipff and Hinz (2009), the experienced mechanical stress and the presence of TGF- β are the two main factors for the development of myofibroblasts. Both of these effects can be used when either differentiation to this phenotype is added to the model or in the size of the exerted contractile forces.

Fourth, the tPA production as explained in section 2.1.2 is considered to be constant throughout time. Since we were not interested in the dynamics of tPA during the later stages of the model,

this assumption had no further consequences. However, tPA may also play a role in processes such as the formation of new blood vessels (angiogenesis). When extensions to this model are made in which such processes are incorporated, the formulation for production of tPA will need to be reevaluated.

Fifth, with respect to cell movement, we have chosen to neglect the directional persistence of cells as shown in Section 2.1.4. This was done in order to emphasize the influence the cytokine gradient has on cell movement. Further research into a formulation of cell movement which both includes the directional persistence and the prominent dependence on the corresponding cytokine may result in an improved modeling technique.

Sixth, the arrival of leukocytes is now modeled as a process which separately determines the amount and location of arriving leukocytes. As shown in Section 2.1.4, the point of entry is chosen according to a uniform distribution on the location of severed blood vessels. This is a major simplification which will need to be reevaluated once the model is expanded to simulate wounds with a larger area. In order to make the model more realistic in this sense, we suggest incorporating assumed locations of severed blood vessels and possibly the process of angiogenesis.

Seventh, the formulation of collagen fibers as a tensor can be exploited further. Besides providing a measure for anisotropy, the density and orientation of fibers can be used to describe a directional variation in elasticity. Naturally, a force acting in the direction in which a fiber is oriented will result in a greater counterforce than a force acting tangential to a fiber's orientation. By taking the directional elasticity into account, the negative effect that anisotropy has on tissue could be modeled directly instead of merely speculating using a measure of anisotropy.

In all, there is room for improvement in various aspects of this model. However, expanding a model by incorporating more effects and relationships may not always improve it. The addition of new components will inevitably introduce more parameters and consequently introduce more uncertainty within the model. Furthermore, the use of certain pairs of parameters may produce the same experimental results which ultimately decreases the significance of these results. In certain aspects it may even be completely unnecessary since we have shown that the phenomena of contraction and contracture associated with dermal wound healing can be modeled with the basic assumptions presented here and show satisfying results.

BIBLIOGRAPHY

- Barocas, V. H. and Tranquillo, R. T. (1997). An anisotropic biphasic theory of tissue-equivalent mechanics: the interplay among cell traction, fibrillar network deformation, fibril alignment, and cell contact guidance. *J Biomech Eng*, 119(2):137–145.
- Clark, R. A. (2014). Chapter 76 - wound repair: Basic biology to tissue engineering. In Lanza, R., Langer, R., and Vacanti, J., editors, *Principles of Tissue Engineering (Fourth Edition)*, pages 1595 – 1617. Academic Press, Boston, fourth edition.
- Cumming, B. (2006). A mathematical model of wound healing and subsequent scarring. Master's thesis, Queensland University of Technology.
- Cumming, B. D., McElwain, D. L., and Upton, Z. (2010). A mathematical model of wound healing and subsequent scarring. *J R Soc Interface*, 7(42):19–34.
- Dallon, J., Sherratt, J., Maini, P., and Ferguson, M. (2000). Biological implications of a discrete mathematical model for collagen deposition and alignment in dermal wound repair. *IMA J Math Appl Med Biol*, 17(4):379–393.
- Dallon, J. C., Sherratt, J. A., and Maini, P. K. (1999). Mathematical modelling of extracellular matrix dynamics using discrete cells: fiber orientation and tissue regeneration. *J. Theor. Biol.*, 199(4):449–471.
- Dallon, J. C., Sherratt, J. A., and Maini, P. K. (2001). Modeling the effects of transforming growth factor-beta on extracellular matrix alignment in dermal wound repair. *Wound Repair Regen*, 9(4):278–286.
- Dziuk, G. and Elliott, C. M. (2007). Finite elements on evolving surfaces. *IMA journal of numerical analysis*, 27(2):262–292.
- Enoch, S. and Leaper, D. J. (2008). Basic science of wound healing. *Surgery (Oxford)*, 26(2):31 – 37.
- Haugh, J. M. (2006). Deterministic model of dermal wound invasion incorporating receptor-mediated signal transduction and spatial gradient sensing. *Biophysical Journal*, 90(7):2297 – 2308.
- Hinz, B. (2006). Masters and servants of the force: The role of matrix adhesions in myofibroblast force perception and transmission. *European Journal of Cell Biology*, 85(3–4):175 – 181.
- van Kan, J., Segal, A., and Vermolen, F. (2008). *Numerical Methods in Scientific Computing*. VSSD.
- Lookingbill, D. and Marks, J. (2000). *Principles of Dermatology*. Saunders.

- McDougall, S., Dallon, J., Sherratt, J., and Maini, P. (2006). Fibroblast migration and collagen deposition during dermal wound healing: mathematical modelling and clinical implications. *Philosophical Transactions of the Royal Society A: Mathematical, Physical and Engineering Sciences*, 364(1843):1385–1405.
- Midwood, K. S., Williams, L. V., and Schwarzbauer, J. E. (2004). Tissue repair and the dynamics of the extracellular matrix. *The International Journal of Biochemistry & Cell Biology*, 36(6):1031 – 1037.
- Murphy, K. E., Hall, C. L., Maini, P. K., McCue, S. W., and McElwain, D. L. (2012). A fibrocontractive mechanochemical model of dermal wound closure incorporating realistic growth factor kinetics. *Bull. Math. Biol.*, 74(5):1143–1170.
- Mutsaers, S. E., Bishop, J. E., McGrouther, G., and Laurent, G. J. (1997). Mechanisms of tissue repair: from wound healing to fibrosis. *The International Journal of Biochemistry & Cell Biology*, 29(1):5 – 17.
- Olsen, L., Maini, P. K., Sherratt, J. A., and Dallon, J. (1999). Mathematical modelling of anisotropy in fibrous connective tissue. *Mathematical Biosciences*, 158(2):145 – 170.
- Olsen, L., Sherratt, J., and Maini, P. (1995). A mechanochemical model for adult dermal wound contraction and the permanence of the contracted tissue displacement profile. *Journal of Theoretical Biology*, 177(2):113–128.
- Olsen, L., Sherratt, J., and Maini, P. (1996). A mathematical model for fibro-proliferative wound healing disorders. *Bulletin of Mathematical Biology*, 58(4):787–808.
- Ross, S. (1996). *Stochastic Processes*. John Wiley & Sons, Inc.
- Tranquillo, R. T. and Murray, J. (1992). Continuum model of fibroblast-driven wound contraction: Inflammation-mediation. *Journal of Theoretical Biology*, 158(2):135 – 172.
- Vermolen, F. J. and Gefen, A. (2012). A semi-stochastic cell-based formalism to model the dynamics of migration of cells in colonies. *Biomech Model Mechanobiol*, 11(1-2):183–195.
- Wesseling, P. (2001). *Principles of Computational Fluid Dynamics*. Lecture Notes in Computer Science. Springer.
- Wipff, P.-J. and Hinz, B. (2009). Myofibroblasts work best under stress. *Journal of Bodywork and Movement Therapies*, 13(2):121 – 127.

A

LISTS OF PARAMETERS

For reproducibility, we present the values of the used parameters in the following tables.

Constant	Value	Description	Source
D_t^{min}	$2.50 \cdot 10^{-2}$	Minimum diffusion tPA.	Cumming et al. (2010).
D_t^{max}	$1.30 \cdot 10^{-3}$	Maximum diffusion tPA.	Cumming et al. (2010).
D_T^{min}	$1.87 \cdot 10^{-2}$	Minimum diffusion TGF- β .	Cumming et al. (2010).
D_T^{max}	$1.90 \cdot 10^{-2}$	Maximum diffusion TGF- β .	Cumming et al. (2010).
D_P	$2.50 \cdot 10^{-2}$	Maximum diffusion TGF- β .	Cumming et al. (2010).
r_p	0.15	Factor of fibrin decay	Cumming et al. (2010).
s_t	0.04	Total tPA production.	Cumming et al. (2010).
α	$1 \cdot 10^{-4}$	Variation in the random walk.	Cumming et al. (2010).
c_{max}	$9.38 \cdot 10^{-4}$	Maximum TGF- β excretion.	Cumming et al. (2010).
c_{fib}	0.10	Fibrin density's influence on TGF- β excretion.	Cumming et al. (2010).
k_1	$1.88 \cdot 10^{-2}$	Minimum collagen synthesis.	Cumming et al. (2010).
k_2	$3.75 \cdot 10^{-2}$	Maximum collagen synthesis.	Cumming et al. (2010).
κ_t	1	Transport tPA into surrounding tissue.	Estimated.
κ_P	1	Transport PDGF into surrounding tissue.	Estimated.
κ_T	1	Transport TGF- β into surrounding tissue.	Estimated.
κ	0.1	Stiffness constant on boundaries.	Estimated.

Constant	Value	Description	Source
β	10	Leukocyte arrival.	Estimated.
μ_l	72	Average life span of leukocytes.	Estimated.
μ_f	120	Average life span of fibroblasts.	Estimated.
n_{thres}	0.5	Threshold receptors for mitosis.	Cumming et al. (2010).
τ_{max}	48	Threshold in time for mitosis.	Cumming et al. (2010).
r_c	$2.50 \cdot 10^{-2}$	Radius of a cell.	Cumming et al. (2010).
r_s	$2.22 \cdot 10^{-2}$	Distance to a cell's force point.	Equation (2.79).
n_f^0	240	Initial number of (myo)fibroblasts.	Estimated.
β_P	1	Rate of unbinding PDGF receptors.	Cumming et al. (2010).
γ_P	5	Rate of binding PDGF receptors.	Cumming et al. (2010).
β_T	1	Rate of unbinding TGF- β receptors.	Cumming et al. (2010).
γ_T	5	Rate of binding TGF- β receptors.	Cumming et al. (2010).
v_l^{max}	1	Maximum velocity for leukocytes.	Cumming et al. (2010).
v_f^{max}	0.38	Maximum velocity for fibroblasts.	Cumming et al. (2010).
k_6	0.10	Influence of fibrin density on cell movement.	Cumming et al. (2010).
γ_l	1	Directional sensitivity to gradient for leukocytes.	Cumming et al. (2010).
γ_f	1	Directional sensitivity to gradient for fibroblasts.	Cumming et al. (2010).
E	$1.60 \cdot 10^{-2}$	Elasticity modulus corresponding to 100 kPA.	Estimated.
ν	0.30	Poisson's ratio.	Estimated.
P_0^f	$2.55 \cdot 10^{-3}$	Temporary force exerted by fibroblasts.	Murphy et al. (2012).
P_0^l	$5.09 \cdot 10^{-3}$	Temporary force exerted by myofibroblasts.	Murphy et al. (2012).
P_{max}	$5.09 \cdot 10^{-3}$	Plastic force exerted by myofibroblasts.	Estimated.
α_τ	1	Rate of formation of plastic force forces.	Estimated.